

# SeSE: A Structural Information-Guided Uncertainty Quantification Framework for Hallucination Detection in LLMs

Xingtao Zhao, Hao Peng, Dingli Su, Xianghua Zeng, Chunyang Liu, Jinzhi Liao, and Philip S. Yu, *Life Fellow, IEEE*

**Abstract**—Reliable uncertainty quantification (UQ) is essential for deploying large language models (LLMs) in safety-critical scenarios, as it enables them to abstain from responding when uncertain, thereby avoiding “hallucinating” falsehoods. However, state-of-the-art UQ methods primarily rely on semantic probability distributions or pairwise distances, overlooking latent semantic structural information that could enable more precise uncertainty estimates. This paper presents Semantic Structural Entropy (SeSE), a principled UQ framework that quantifies the inherent semantic uncertainty of LLMs from a structural information perspective for hallucination detection. SeSE operates in a zero-resource manner and is applicable to both open- and closed-source LLMs, making it an “off-the-shelf” solution for new models and tasks. Specifically, to effectively model semantic spaces, we first develop an adaptively sparsified directed semantic graph construction algorithm that captures directional semantic dependencies while automatically pruning unnecessary connections that introduce negative interference. We then exploit latent semantic structural information through *hierarchical abstraction*: SeSE is defined as the structural entropy of the optimal semantic encoding tree, formalizing intrinsic uncertainty within semantic spaces after optimal compression. A higher SeSE value corresponds to greater uncertainty, indicating that LLMs are highly likely to generate hallucinations. In addition, to enhance fine-grained UQ in long-form generation—where existing methods often rely on heuristic sample-and-count techniques—we extend SeSE to quantify the uncertainty of individual claims by modeling their random semantic interactions, providing theoretically explicable hallucination detection. Extensive experiments across 29 model-dataset combinations show that SeSE significantly outperforms advanced UQ baselines, including strong supervised methods and the recently proposed KLE. These findings highlight the importance of semantic structural information for precise UQ in LLMs, establishing SeSE as a reliable framework for assessing the trustworthiness of LLM-based systems<sup>1</sup>.

**Index Terms**—Large language models, uncertainty quantification, structural entropy, hallucination detection

## I. INTRODUCTION

Xingtao Zhao and Hao Peng are with the School of Cyber Science and Technology, Beihang University, Beijing 100191, China; (e-mail: xtaozhao@buaa.edu.cn; penghao@buaa.edu.cn);

Dingli Su and Xianghua Zeng are with the School of Computer Science and Engineering, Beihang University, Beijing 100191, China. (e-mail: sudingli@buaa.edu.cn; zengxianghua@buaa.edu.cn);

Chunyang Liu is with the Didi Chuxing, Beijing 100193, China (e-mail: liuchunyang@didiglobal.com)

Jinzhi Liao is with Laboratory for Big Data and Decision, National University of Defense Technology, Changsha 410073, China. (e-mail: liaojinzhi12@nudt.edu.cn).

Philip S. Yu is with the Department of Computer Science, University of Illinois Chicago, Chicago, IL 60607 USA. (e-mail: psyu@uic.edu).

<sup>1</sup>The code and data is available: <https://github.com/SELGroup/SeSE>

**L**ARGE language models (LLMs) have been widely adopted across various fields, including spatio-temporal data modeling [1], sentiment analysis [2] and recommender systems [3]–[5], due to their impressive general intelligence. However, a key limitation of LLMs is *hallucinations* [6]—the generation of plausible yet incorrect statements, which hinders their deeper adoption in real-world [7]. Despite extensive research having sought to eliminate hallucinations by verifying model outputs against evidence retrieved from external knowledge bases [8]–[10], they are often domain-specific and fail to address hallucinations beyond pure fact-checking [7]. A promising direction for avoiding hallucinations is uncertainty quantification (UQ) [11], [12]. As shown in Figure 1, UQ mines uncertainty information and assigns an uncertainty score to the model when answering a given input. A low score suggests LLM responses for a given input are acceptable, whereas a high score should trigger LLMs to abstain from responding and warn users of potential hallucinations.

But the open-ended nature of LLM generation hinders the direct application of traditional UQ methods [13], which treat LLM outputs as conventional autoregressive sequences and consider only their lexical uncertainty. Since response correctness fundamentally depends on semantics in most LLM applications, and distinct token sequences can convey identical meanings, uncertainty in the semantic space is a more essential indicator of response trustworthiness than lexical uncertainty. To address this issue, semantic entropy (SE) [14] and its subsequent extensions [15]–[17] quantify uncertainty at the semantic rather than token level, achieving state-of-the-art (SOTA) performance in UQ tasks.

However, current semantic UQ methods exhibit three intrinsic limitations. **First, they ignore the structural information embedded within semantic spaces.** As illustrated in Figure 2 (2), real-world semantic spaces are often hierarchically organized—substructures recursively contain finer sub-substructures. According to the “Compositional Similarity” principle [18], identifying the hierarchical structure enables more precise UQ, as differences among substructures may help distinguish superficially similar semantic spaces. SE is a binary, one-cut measurement that considers only the uncertainty of the distribution over semantic clusters. Kernel language entropy (KLE) [17], a recent follow-up of SE, computes the von Neumann entropy of semantic graph kernels, but the decomposed semantic substructures are non-hierarchical and any substructure can be compared with any other. This violates the “Compositional Similarity” principle and limits the precision of UQ.

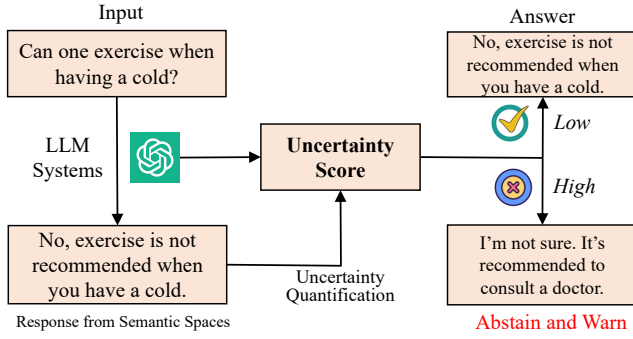


Figure 1: Illustration of LLM UQ for avoiding hallucinating.

**Second, existing semantic UQ methods often represent semantic spaces using suboptimal undirected, complete graphs [17], [19].** Undirected graphs capture only symmetric similarity between responses, implicitly assuming that the similarity from A to B equals that from B to A. However, in semantic studies, entailment relations are directionally asymmetric [20]; for example, “apples” entails “green apple”, but not vice versa. Ignoring this directionality discards crucial semantic logic and leads to irreversible information loss. Moreover, complete graphs may contain numerous low-value edges (e.g., edges with near-zero weights) that obfuscate core semantic structures and reduce computational efficiency. Existing sparsification approaches primarily fall into two categories: (i) removing redundant inter-cluster edges through pairwise semantic equivalence assessment [16], [17], which has a worst-case time complexity  $O(n^2)$  and incurs substantial computational cost; and (ii) relying on domain knowledge to manually set pruning thresholds [21]–[23], which fails to generalize to task-specific semantics.

**Thirdly, granular uncertainty estimation for long-form generations remains challenging.** Although existing semantic UQ methods have made notable progress in short-form settings where generations typically consist of one or two sentences [14]–[17], [24], real-world LLM applications predominantly involve long-form generations that interleave numerous true or false claims. Recent works [22], [25]–[27] have begun to evaluate the factual accuracy of individual claim outputs based on the concept of self-consistency [25]. However, they rely purely on heuristic sample-and-count techniques, which fail to capture more sophisticated semantic relationships between claims and responses.

To address these challenges, we present SeSE, a principled zero-resource UQ framework that quantifies semantic uncertainty from the perspective of structural information theory for LLM hallucination detection. SeSE is self-contained: it relies solely on sampled LLM responses and can thus be applied to both open-source and proprietary LLMs without requiring any additional training or external tools. Our framework offers three key advancements: **First**, we develop an adaptively sparsified directed semantic graph construction algorithm (AS-DSG) to effectively represent semantic spaces. The directed semantic graph, with edges weighted by directional entailment probabilities, captures both semantic directionality and similarity. Inspired by neighbor network construction in cancer cell analysis [28], AS-DSG employs an adaptive graph sparsification mechanism that minimizes the

one-dimensional structural entropy to prune the directed graph into an optimal  $k$ -nearest neighbor (kNN) graph, thereby reducing redundancy. This procedure does not require manually setting  $k$  or costly pairwise comparisons, adaptively prunes trivial edges, and preserves core semantic structure. **Then**, we fully capture semantic structural information by constructing the *hierarchical abstraction* using an encoding tree. SeSE is defined as the structural entropy of the  $K$ -dimensional optimal encoding tree derived from the constructed semantic graph based on the principle of structural entropy minimization [29]. SeSE thus quantifies the residual uncertainty within semantic spaces after optimal compression. Semantic spaces with clear regularities exhibit low entropy (low uncertainty), whereas disordered spaces resist compression and yield high entropy (high uncertainty). **Furthermore**, we extend SeSE to quantify claim-level uncertainty in long-form generation, improving granular UQ by considering fine-grained semantic dependencies within semantic spaces. Following prior work on long-form generation decomposition [27], [30], we segment LLM outputs into atomic claims and construct a response-claim bipartite graph to model their semantic interactions. The SeSE of a claim is defined as the uncertainty of reaching that claim through random walks on the response-claim graph, offering both theoretical and empirical advantages over conventional sample-and-count techniques. Claims with low SeSE lie within core semantic regions, implying they are frequently accessed during the LLM’s sequence generation and are thus highly likely to be factual. Conversely, claims with high SeSE occupy peripheral semantic positions, increasing their likelihood of being associated with hallucinations. In summary, the main contributions of this paper are:

- We propose SeSE, a principled and self-contained UQ framework applicable to both open- and closed-source LLMs. To the best of our knowledge, this is the *first* work to incorporate semantic structural information into UQ.
- We develop an adaptively sparsified directed semantic graph construction algorithm (AS-DSG) that captures directional semantic relationships while adaptively pruning insignificant edges to reduce interference.
- Based on structural information theory, we quantify the inherent uncertainty within the semantic space of LLMs. We refine naive structural entropy to enable hierarchical abstraction under asymmetric connections by introducing an optimized redefinition and an associated optimization operator.
- We extend SeSE to provide enhanced granular UQ in long-form generation by accounting for fine-grained semantic interactions, offering both theoretical and empirical advantages over existing heuristic techniques.
- We conducted comprehensive experiments across 29 scenarios, encompassing both open- and closed-source LLMs and multiple free-form QA datasets with varying generation lengths. Experimental results highlight SeSE’s superior performance over existing SOTA UQ baselines.

## II. PRELIMINARIES AND PROBLEM FORMULATION

In this section, we first define the LLM uncertainty quantification problem in Section II-A, then present the basic concepts

of predictive uncertainty (Section II-C) and naive structural entropy (Section II-B).

### A. Problem Statement

Given a pre-trained LLM  $\mathcal{M}$ , SeSE takes as input the user query  $x$  and  $N$  responses  $\mathcal{R}(\cdot|X) = \{r_{T=t}^1, \dots, r_{T=t}^N\}$  that are sampled from  $\mathcal{M}$  at temperature  $T = t$ , and outputs an uncertainty score  $U(x)$  that is positively correlated with the probability of the best generation (i.e., greedy-decoded response)  $r_{T=0}$  being hallucination. LLM-based systems can use  $U(x)$  as a quantitative indicator to assess the trustworthiness of  $\mathcal{M}$ 's response to  $x$ .

### B. Naive Structural Entropy

Structural entropy is an extension of Shannon entropy for measuring the uncertainty of a graph under hierarchical abstraction. It represents the minimum code length required to describe a graph's hierarchy during random walks [31]. An encoding tree with the minimum structural entropy captures the natural structure of the semantic space.

**Definition 1** (Encoding tree). *Given the graph  $G$ , the encoding tree  $\mathcal{T}$  for  $G$  is a rooted tree satisfying the following conditions: (1) The root node  $\lambda$  contains all nodes in  $G$ ,  $\mathcal{T}_\lambda = V$ . Each node  $\alpha \in \mathcal{T}$  represents a partition of responses  $\mathcal{T}_\alpha \subseteq V$ . For any leaf node  $\gamma$ ,  $\mathcal{T}_\gamma$  contains a single response from  $V$ . (2) Each non-leaf node  $\alpha$  has a nonempty set of immediate successors denoted as  $\beta_0, \beta_1, \dots, \beta_l$ . The collection of subsets  $\{\mathcal{T}_{\beta_0}, \mathcal{T}_{\beta_1}, \dots, \mathcal{T}_{\beta_l}\}$  forms a partition of  $\mathcal{T}_\alpha$ .*

**Definition 2** (One-dimensional structural entropy). *The one-dimensional structural entropy of  $G$  reflects the dynamical uncertainty of  $G$  based on random walks, defined as:*

$$H^1(G) = - \sum_{v \in V} \frac{d_v}{\text{vol}(G)} \log_2 \frac{d_v}{\text{vol}(G)}, \quad (1)$$

where  $d_v$  is the sum of the weights of  $v$ 's connected edges, and  $\text{vol}(G) = \sum_{v \in V} d_v$  is the volume of  $G$ .

**Definition 3** (Structural Entropy of the Encoding Tree  $\mathcal{T}$ ). *The structural entropy of  $G$  under the hierarchical abstraction represented by the encoding tree  $\mathcal{T}$  is defined as:*

$$H^\mathcal{T}(G) = \sum_{\alpha \in \mathcal{T}, \alpha \neq \lambda} H^\mathcal{T}(G; \alpha), \quad (2)$$

$$H^\mathcal{T}(G; \alpha) = - \frac{g_\alpha}{\text{vol}(G)} \log_2 \frac{\mathcal{V}_\alpha}{\mathcal{V}_{\alpha^-}}, \quad (3)$$

where  $g_\alpha$  is the sum of weights of edges from the nodes in  $\mathcal{T}_\alpha$  to those outside of  $\mathcal{T}_\alpha$ ,  $\mathcal{V}_\alpha = \sum_{v \in \mathcal{T}_\alpha} d_v$  is the volume of  $\mathcal{T}_\alpha$ , and  $\alpha^-$  is the parent node of  $\alpha$ .

### C. Predictive Uncertainty.

LLM generation can be viewed as a classification problem with extremely high dimension [19]. In classification, uncertainty is typically measured by predictive entropy (PE) [14]. The predictive entropy of the output random variable  $Y$  with realization  $y$  given  $x$  is formally defined as  $H(Y | x) = - \int p(y | x) \log(p(y | x)) dy$ , which becomes the following uncertainty score in natural language generation:

$$U(x) = H(S | x) = - \sum_s p(s | x) \log(p(s | x)). \quad (4)$$

Here, the summation covers all possible generated sequences  $s \in S$ . High entropy indicates that many potential outputs have similar likelihoods, suggesting LLMs possess significant uncertainty about the correct answer and are highly likely to generate hallucinations. Conversely, low entropy implies a heavily concentrated output distribution, implying that LLMs probably possess relevant knowledge of correct answers.

Predictive uncertainty is occasionally characterized as total uncertainty, comprising both epistemic and aleatoric uncertainty [11]. Aleatoric uncertainty (data uncertainty) represents the irreducible uncertainty inherent in the data distributions, whereas epistemic uncertainty (model uncertainty) reflects the knowledge limitations of LLMs. Following most prior work, we focus on estimating total uncertainty, since both components jointly contribute to hallucinations. Although the distinction between these uncertainties would certainly enhance the performance of our proposed SeSE, we leave this extension to future work.

## III. METHODOLOGY

This section provides an overview of our proposed SeSE, as illustrated in Figures 2—3. First, we formally define the semantic space and directed structural entropy in Section III-A, which form the theoretical foundation for SeSE. Then, we introduce the pipeline of SeSE for sentence-level generation ( $16 \pm 11$  tokens, mean  $\pm$  s.d.) in Section III-B. Specifically, Section III-B1 specifies the sampling setup; Section III-B2 details the semantic graph construction algorithm; and Section III-B3 formally defines SeSE and introduces the proposed directed structural entropy minimization method. Finally, we elaborate on how SeSE operates at the claim-level in long-form generation ( $142 \pm 25$  tokens) in Section III-C.

### A. Semantic Space and Directed Structural Entropy

A semantic space models a set of interacting semantic entities and their dynamic relationships within a specific context. Note that each context defines a unique semantic space, i.e., identical semantic entities may exhibit different relationships across different contexts. Formally, such systems can be described using two equivalent mathematical frameworks: a graph-theoretic structure and an algebraic matrix model. We first define the graph model as follows:

**Definition 4** (Graph Model of a Semantic Space). *A semantic space is formulated as a directed weighted graph  $G_{dir} = (V, E, W)$ , where:*

- $V$  is a finite set of vertices representing semantic entities.
- $E \subseteq V \times V$  is a set of directed edges encoding interactions between vertices.
- $W : E \rightarrow \mathbb{R}^{\geq 0}$  is a context-specific weight function such that  $W(i, j) > 0$  quantifies the interaction strength from semantic entities  $i$  to entity  $j$  within specific context. If  $(i, j) \notin E$ , then  $W(i, j) = 0$ .

Weights can be instantiated using text embedding models, natural language inference models, or a weighted combination of the two, ensuring  $W(i, j) \geq 0$  for all  $i, j$ .

The algebraic model enables the analysis of semantic uncertainty using linear algebra and spectral methods, whose formal definition is as follows:

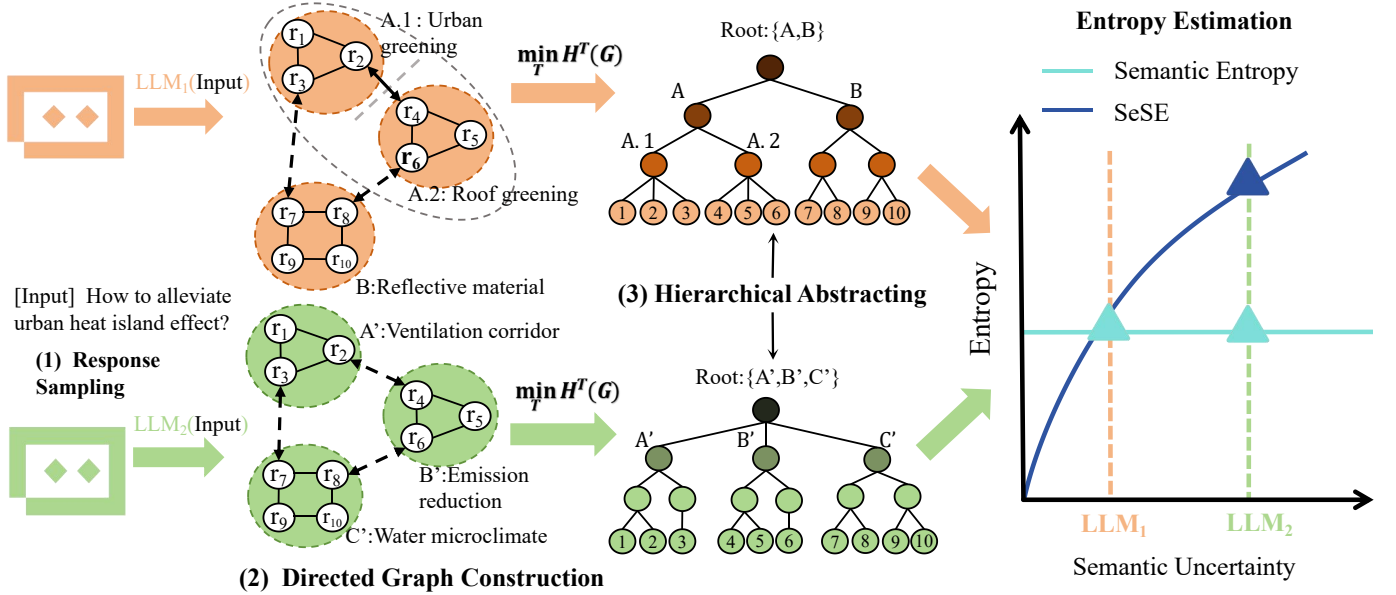


Figure 2: Overview of SeSE in sentence-length generation. For the sake of the example, we assume that the probabilities of each semantic cluster in (b) are equal, i.e.,  $p(c_i|\text{input}) = p(c'_i|\text{input}), \forall c \in C$ . Although the semantic structure of LLM<sub>1</sub> is more regular and its uncertainty should be lower (i.e., LLM<sub>1</sub> is quite certain that “urban greening” is a good answer), the semantic entropy fails to distinguish the differences and yields identical uncertainty scores due to their initially similar semantic spaces. In contrast, SeSE explicitly considers structural information via constructed semantic graphs, where concept “A” comprises two 3-level substructures “A.1” and “A.2”, thus correctly identifying that LLM<sub>1</sub> should be assigned lower uncertainty.

**Definition 5** (Algebraic Model of a Semantic Space). A semantic space can be equivalently represented by a non-negative matrix  $A \in \mathbb{R}_{\geq 0}^{|V| \times |V|}$ , where each element  $a_{i,j} = W(i,j)$  denotes the interaction from entity  $i$  to  $j$ . The matrix  $A$  thus fully preserves the structure of  $G_{dir}$ .

To address the limitations imposed by undirected constraints in the naive structural entropy [29], [32], [33], we define the high-dimensional structural entropy for directed graphs, enabling an accurate representation of directional semantic information in the semantic space. We first present the following theorem, forming the basis for the definition of directed structural entropy.

**Theorem 1.** Given a directed graph  $G_{dir}$  with non-negative edge weights and its corresponding matrix  $A$ , if  $A$  is an irreducible stochastic matrix, then  $G_{dir}$  possesses a unique stationary distribution  $\pi^\top$  satisfying  $\pi^\top A = \pi^\top$ . This distribution corresponds to the unique eigenvector associated with the dominant eigenvalue 1 of the adjacency matrix  $A$ .

Proof of this theorem based on the Perron-Frobenius theorem is provided in Appendix VIII-A.

Therefore, to ensure the constructed directed semantic graph  $G_{dir}$  possesses a unique stationary distribution  $\pi$ —a prerequisite for defining directed structural entropy—we define the **adjusting** operator. As presented in Algorithm 1, this operator serves two purposes: (i) ensuring  $G_{dir}$  is irreducible by guaranteeing a directed path exists between any pair of vertices; and (ii) normalizing edge weights such that the weighted out-degree of each vertex sums to 1, thereby transforming  $G_{dir}$  into a Markov chain conducive to a random walk. Specifically, we first identify the graph’s strongly connected components

(SCCs) using Tarjan’s algorithm [34]. We then introduce directed edges with minimal weights to establish connectivity between these components. Finally, for each vertex  $v \in V$ , we normalize the weights of its outgoing edges by dividing each edge weight by the vertex’s weighted out-degree sum.

---

#### Algorithm 1: Adjusting Operator

---

**Input:** A directed weighted graph  $G_{dir} = (V, E, W)$  with non-negative edge weights  
**Output:** A strongly connected directed graph  $G'_{dir}$  with normalized edge weights

```

// SCCs decomposition
1  $SCCs \leftarrow \text{Tarjan}(G_{dir})$  [34],  $G_{SCC} = (V_{SCC}, E_{SCC})$ 
// make  $G_{SCC}$  strongly connected
2  $sources \leftarrow$  SCCs with no incoming edges in  $G_{SCC}$ 
3  $sinks \leftarrow$  SCCs with no outgoing edges in  $G_{SCC}$ 
4 if  $|V_{SCC}| > 1$  then
5   foreach sink SCC  $S_{sink}$  do
6     foreach source SCC  $S_{source}$  do
7       if there’s no path from  $S_{sink}$  to  $S_{source}$  then
8         Add a minimum-weight edge from  $S_{sink}$  to  $S_{source}$ 
// out-degree normalization
9 foreach edge  $(v_i, v_j) \in E$  do
10    $W(v_i, v_j) \leftarrow W(v_i, v_j) / \sum_{(v_i, v_k) \in E} W(v_i, v_k)$ 
11 return  $G'_{dir} \leftarrow G_{dir}$ 

```

---

For the adjusted semantic graph  $G'_{dir} = (V, E', W')$ , we compute the stationary distribution  $\pi$  over all vertices

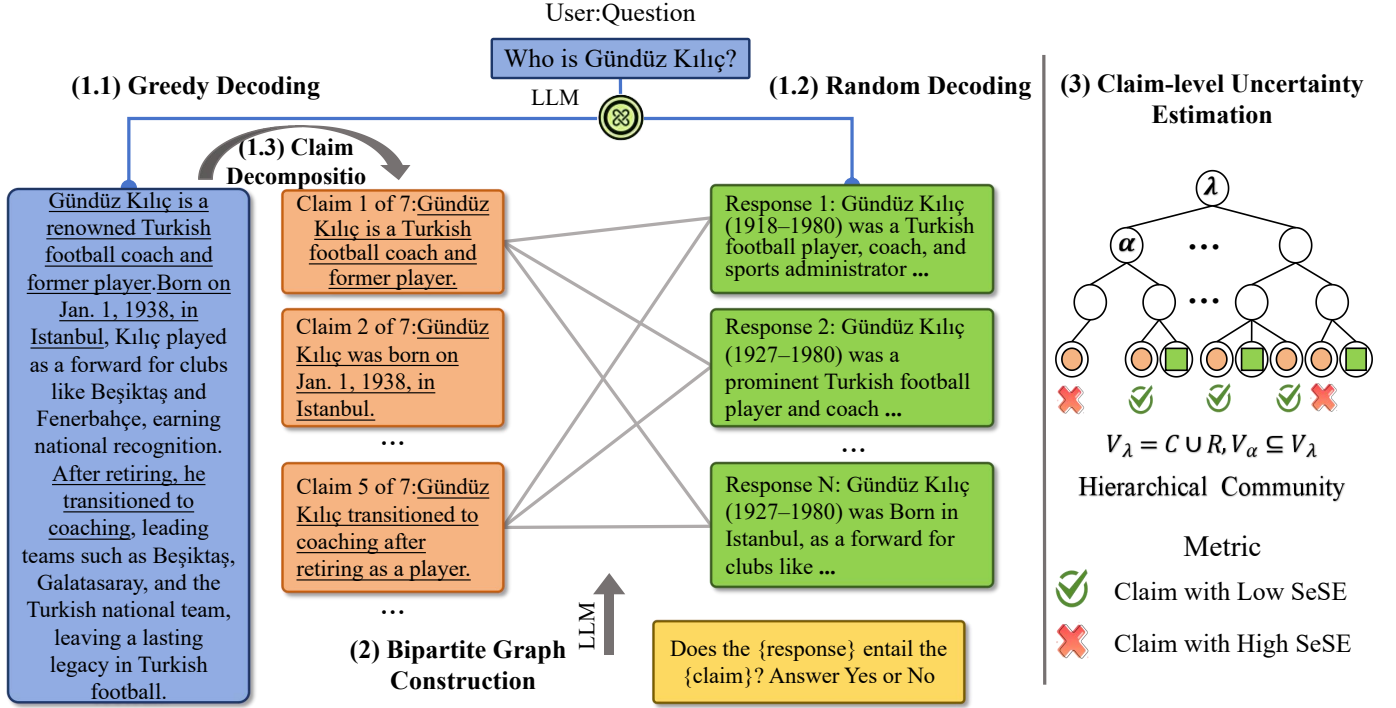


Figure 3: Overview of SeSE in long-form generation. We decompose the generated long-form response into atomic claims. SeSE quantifies the uncertainty of individual claims by modeling their random semantic interactions, and hallucination is indicated by a high SeSE value associated with that claim in the constructed bipartite response-claim graph.

and define the one-dimensional directed structural entropy as follows:

$$H^1(G'_{dir}) = - \sum_{v \in V} \pi(v) \cdot \log_2 \pi(v), \quad (5)$$

where  $\pi(v)$  denotes the stationary probability of vertex  $v$  in  $G'_{dir}$ . Using the stationary distribution  $\pi$ , we redefine  $g_\alpha$  and  $V_\alpha$  for each non-root node  $\alpha$  in the encoding tree  $\mathcal{T}_{dir}$  of  $G'_{dir}$ , and its assigned entropy as follows:

$$V_\alpha = \sum_{v_i \in V} \sum_{v_j \in V_\alpha} [\pi(v_i) \cdot W'(v_i, v_j)], \quad (6)$$

$$g_\alpha = \sum_{v_i \notin V_\alpha} \sum_{v_j \in V_\alpha} [\pi(v_i) \cdot W'(v_i, v_j)], \quad (7)$$

$$H^{\mathcal{T}_{dir}}(G'_{dir}; \alpha) = - \frac{g_\alpha}{\text{vol}(G'_{dir})} \cdot \log_2 \frac{V_\alpha}{V_\alpha^-}, \quad (8)$$

where the volume of  $G'_{dir}$  is redefined as the sum of in-degrees and out-degrees of all vertices:

$$\text{vol}(G'_{dir}) = \sum_{v \in V} (d_v^+ + d_v^-), \quad (9)$$

where  $d_v^+$  and  $d_v^-$  denote the weighted out-degree and in-degree of vertex  $v$ , respectively. Thus, the directed structural entropy of  $G'_{dir}$  is redefined as follows:

$$H^{\mathcal{T}_{dir}}(G'_{dir}) = \sum_{\alpha \in \mathcal{T}_{dir}, \alpha \neq \lambda} H^{\mathcal{T}_{dir}}(G'_{dir}; \alpha), \quad (10)$$

### B. SeSE for Sentence-length Generation

While semantic entropy aims to estimate the LLM's uncertainty in the semantic space, it fails to capture the intrinsic semantic structure. Therefore, SeSE extends the simple

Shannon entropy of semantic clusters to the  $K$ -dimensional structural entropy of directed semantic graphs, enabling more precise uncertainty estimation. At a high level, this involves three steps: response sampling, semantic graph construction and hierarchical abstraction.

1) *Response Sampling*: Unlike white-box UQ approaches that require access to the internal token probabilities of LLMs, SeSE only needs a set of sampled answers as input, thus having broader applicability. Given the context  $x$  as input to  $\mathcal{M}$ , we sample two types of responses from  $\mathcal{M}$ : a single greedy-decoded answer  $r_{T=0}$  and a set of  $N$  stochastically sampled answers  $\mathcal{R}(\cdot | x) = \{r_{T=1}^1, \dots, r_{T=1}^N\}$ . Responses in  $\mathcal{R}$  are generated at a temperature of  $T = 1$  using nucleus (top- $P$ ) sampling [35] and top- $K$  sampling [36], with parameters  $P = 0.95, K = 20$ . The greedy decoding response  $r_{T=0}$ , obtained by setting  $T = 0, P = 1, K = 20$ , serves as the model's most confident answer and is used for accuracy evaluation. The temperature parameter  $T$  controls the stochasticity of the LLM's output by scaling the logits over the next token. A lower temperature value amplifies the probability of initial high-probability tokens.  $T = 1$  preserves the model's original output distribution, whereas  $T = 0$  results in deterministic decoding by always selecting the highest probability token. We default to setting the sample size  $N = 10$  and the relevant hyperparameter analysis is presented in Section V-D1. The prompt template can be found in Appendix VIII-F.

2) *Semantic Graph Construction*: Prior studies have generally constructed undirected, fully connected semantic graphs, which neglect inherently directional semantic information and often introduce numerous redundant connections. To capture directional relationships between responses and elim-

**Algorithm 2:** Proposed AS-DSG

---

**Input:** Context  $x$ , the sampled response set  $\mathcal{R}(\cdot | x) = \{r_{T=1}^1, \dots, r_{T=1}^N\}$ , NLI model

**Output:** An irreducible, directed sparsified semantic graph  $G_{dir}^* = (V, E, W)$  with normalized edge weights

// **pairwise entailment measurement**

- 1 Initialize a weight matrix  $A \in \mathbb{R}^{N \times N}$  to 0
- 2 **foreach** ordered pair  $(r^i, r^j) \in \mathcal{R} \times \mathcal{R}$  **do**
- 3     **if**  $i \neq j$  **then**
- 4         compute  $P_{NLI}(r^i \rightarrow r^j | x)$  via Eq. 11
- 5         set  $A_{i,j}$  via Eq. 12
- 6     **end**
- 7 **end**

// **initialize semantic graph**

- 8  $G_{dir} \leftarrow A$
- 9 // **graph sparsification**
- 9 **for**  $k = 1$  to  $N - 1$  **do**
- 10     construct  $G_k$  as the  $k$ NN graph from  $G_{dir}$
- 11      $G_k \leftarrow \text{Adjusting}(G_k)$  // apply Algorithm 1
- 12     calculate  $H^1(G_k)$  via Eq. 5
- 13 **end**
- 14  $k^* \leftarrow \arg \min_k \{H^1(G_k)\}$
- 15 **return**  $G_{dir}^* \leftarrow G_{k^*}$

---

inate interference from irrelevant connections, we propose an adaptively sparsified directed semantic graph construction algorithm (AS-DSG). The main input to AS-DSG is the response set  $\mathcal{R}$  sampled in Section III-B1, and its output is an irreducible (i.e., strongly connected), directed sparsified semantic graph  $G_{dir}^* = (V, E, W)$  with normalized edge weights. As presented in Algorithm 2, AS-DSG proceeds in two stages: pairwise entailment measurement and graph sparsification.

*Pairwise entailment measurement:* First, we perform pairwise semantic entailment measurement to obtain the mathematical representation of the semantic space, which facilitates the subsequent analysis of semantic uncertainty (lines 2-7 in Algorithm 2). Most existing text embedding models exhibit limitations in measuring contextual semantic similarity. Given a context  $x$  and a response  $r$ , they typically generate an embedding for the whole concatenated sequence  $E(x \oplus r)$  instead of a context-conditioned embedding  $E(r|x)$ . In contrast, natural language inference (NLI) models have been demonstrated to effectively analyze contextually semantic relationships between texts [16].

To preserve semantic directional information, we employ the NLI model DeBERTa-v3-large-mnli<sup>2</sup> to perform pairwise entailment measurements on the sampled response set  $\mathcal{R}$ . For each ordered pair  $(r^i, r^j) \in \mathcal{R} \times \mathcal{R}$  with  $r^i \neq r^j$ , we construct a premise-hypothesis pair  $(x \oplus r^i, x \oplus r^j)$ . Given each pair as input, the NLI model outputs corresponding logits for three classes: entailment, neutral, and contradiction, capturing the directional semantic relationships from  $x \oplus r^i$  (premise) to  $x \oplus r^j$  (hypothesis). We then apply the softmax function  $\sigma(\cdot)$

to these logits to obtain a probability distribution  $P_{NLI}(r^i \rightarrow r^j | x)$ , which is denoted as a three-element tuple:

$$[p_e(r^i \rightarrow r^j | x), p_n(r^i \rightarrow r^j | x), p_c(r^i \rightarrow r^j | x)] = \sigma(NLI(x \oplus r^i, x \oplus r^j)). \quad (11)$$

Here,  $p_e(r^i \rightarrow r^j | x)$ ,  $p_n(r^i \rightarrow r^j | x)$ ,  $p_c(r^i \rightarrow r^j | x)$  denote the semantically equivalent, irrelevant, or contradictory probabilities from  $r^i$  to  $r^j$  conditioned on the context  $x$ , respectively.

To this end, an asymmetric adjacency matrix  $A$  is derived for constructing the directed semantic graph  $G_{dir} = (V, E, W)$ . The  $V = \mathcal{R}$  denotes the set of sampled responses and  $E$  is the set of directed edges with weights defined by the context-specific function  $W$ . The edge weight from node  $i$  to node  $j$  is defined as:

$$W(r^i, r^j) = A_{i,j} = \omega \cdot P_{NLI}(r^i \rightarrow r^j | x), \quad (12)$$

where  $\omega = (1, \frac{1}{2}, 0)^\top$  is a weight vector. This value  $A_{i,j}$  represents the probability of a directed semantic transformation from response  $r^i$  to  $r^j$ . Unless the  $r^i$  and  $r^j$  are completely identical,  $A_{i,j}$  is not necessarily equal to  $A_{j,i}$ . This asymmetry distinguishes  $G_{dir}$  from traditional undirected semantic graphs, which often impose symmetry by averaging bidirectional edge weights (e.g.,  $\frac{A_{i,j} + A_{j,i}}{2}$ ). Such averaging can obscure the directionality of semantic relations and result in information loss.

*Graph sparsification:* While constructing a semantic entailment graph to represent all inter-node relationships is reasonable, the resulting initial graph is fully connected (i.e., all nodes belong to a single class). This configuration introduces numerous insignificant connections that obscure the underlying semantic structure. To address this, we propose an adaptive sparsification mechanism (lines 12–16 in Algorithm 2). Based on structural information theory [31], we sparsify the graph  $G_{dir}$  into a  $k$ NN graph  $G_k$  by minimizing its one-dimensional structural entropy. Notably,  $k$  is determined adaptively based on structural entropy, requiring no manual specification. Specifically, the sparsification procedure involves treating each sampled response  $r \in \mathcal{R}$  as a central vertex and retaining only the highest  $k$  outgoing edge weights to construct a candidate  $k$ NN graph  $G_k$  and compute corresponding one-dimensional structural entropy  $H^1(G_k)$ . (The adjusting operator ensures the existence and uniqueness of the stationary distribution  $\pi$  of  $G_k$ ). We evaluate  $H^1(G_k)$  across a reasonable range of  $k$  values, select optimal parameter  $k^*$  that satisfies the following inequality:

$$H^1(G_{k^*-1}) \geq H^1(G_{k^*}) \leq H^1(G_{k^*+1}), \quad (13)$$

and output  $G_{k^*}$  as the sparsified semantic graph  $G_{dir}^*$ , which preserves the most useful structural information from the initial complete graph.

3) *Hierarchical Abstraction:* Finally, we employ an encoding tree to formalize the concept of hierarchical abstraction. Minimizing a graph’s uncertainty can be achieved by identifying an encoding tree with minimal structural entropy [31]. The optimal encoding tree  $\mathcal{T}^*$  of  $G_{dir}^*$  with the minimum structural entropy quantifies the inherent uncertainty remaining in the

<sup>2</sup><https://huggingface.co/khalidalt/DeBERTa-v3-large-mnli>

**Algorithm 3:** Hierarchical Abstraction

---

**Input:** the sparsified directed semantic graph  $G_{dir}^*$ ,  
 $K > 1$

**Output:** the  $K$ -dimensional optimal encoding tree  $\mathcal{T}^*$

- 1 Initialize a one-dimensional encoding tree  $\mathcal{T}$
- 2 **while** tree height  $h < K$  **do**
- 3     **foreach** sibling nodes  $\alpha, \beta \in \mathcal{T}$  **do**
- 4          $\alpha^*, \beta^* \leftarrow \arg \max \Delta SeSE_{\alpha, \beta}^{op_{mer}}$  via Eq. 16
- 5     **end**
- 6     **if**  $\Delta SeSE_{\alpha, \beta}^{op_{mer}} > 0$  **then**
- 7          $\mathcal{T} \leftarrow op_{mer}(\mathcal{T}, \alpha^*, \beta^*)$ , continue
- 8     **end**
- 9     **foreach** sibling nodes  $\alpha, \beta \in \mathcal{T}$  **do**
- 10          $\alpha^*, \beta^* \leftarrow \arg \max \Delta SeSE_{\alpha, \beta}^{op_{com}}$  via Eq. 16
- 11     **end**
- 12     **if**  $\Delta SeSE_{\alpha, \beta}^{op_{com}} > 0$  **then**
- 13          $\mathcal{T} \leftarrow op_{com}(\mathcal{T}, \alpha^*, \beta^*)$ , continue
- 14     **end**
- 15     **break**
- 16 **end**
- 17 **return**  $\mathcal{T}^* \leftarrow \mathcal{T}$

---

semantic space after optimal compression. Therefore, we define SeSE as the total entropy over the optimal  $K$ -dimensional encoding tree  $\mathcal{T}^*$ , which is the natural hierarchical partitioning of  $G_{dir}^*$ . Formally,

$$\mathcal{T}^* = \arg \min_{\forall \mathcal{T}: \text{height}(\mathcal{T}) \leq K} (H^{\mathcal{T}}(G_{dir}^*)), \quad (14)$$

$$SeSE(G_{dir}^*) = \sum_{\alpha \in \mathcal{T}^*, \alpha \neq \lambda} H^{\mathcal{T}^*}(G_{dir}^*; \alpha). \quad (15)$$

To build the optimal encoding tree  $\mathcal{T}^*$ , we design an efficient structural entropy optimization algorithm. Specifically, leveraging the “merging” ( $op_{mer}$ ) and “combining” ( $op_{com}$ ) operators introduced in [31], we design an efficient structural entropy minimization algorithm for hierarchical abstraction, which is detailed in Algorithm 3. Specifically, the operators  $op_{mer}$  and  $op_{com}$  act upon sibling nodes  $\alpha, \beta \in \mathcal{T}$  that share a common parent. Let  $\mathcal{T}_{\alpha, \beta}$  be the encoding tree obtained after executing the “merging” or “combining” operator on  $\alpha$  and  $\beta$ ; we define the resulting entropy variation as:

$$\Delta SeSE_{\alpha, \beta}^{op} = H^{\mathcal{T}}(G) - H^{\mathcal{T}_{\alpha, \beta}}(G_{dir}^*), \quad (16)$$

which can be calculated using Eq. 10. First, we initialize a one-dimensional encoding tree  $\mathcal{T}$  for  $G_{dir}^*$ : 1) We generate a root node  $\lambda$  as layer 0, representing the entire semantic space, i.e.,  $\mathcal{T}_{\lambda} = \mathcal{R}$ ; 2) For each response  $r \in \mathcal{R}$ , we generate a leaf node  $\gamma$  with  $\mathcal{T}_{\gamma} = \{r\}$  and assign it as a child node of  $\lambda$ , i.e.,  $\gamma^- = \lambda$ . Subsequently, we iteratively optimize the encoding tree  $\mathcal{T}$  to  $K$  layers to construct the optimal  $K$ -dimensional encoding tree  $\mathcal{T}^*$ . In each iteration, we traverse all sibling node pairs in  $\mathcal{T}$  and greedily execute the operator  $op_{mer}$  or  $op_{com}$ , selecting the operation that maximizes the decrease of structural entropy while ensuring the tree height remains below  $K$ . The iterative procedure terminates when no sibling pair satisfies  $\Delta SeSE_{\alpha, \beta}^{op} > 0$  or the tree height exceeds  $K$ , at which point we output the optimal encoding tree  $\mathcal{T}^*$ . Each level

of  $\mathcal{T}^*$  reflects the optimal progressive semantic partitioning of semantic spaces. Lower layers correspond to fine-grained partitions that capture subtle distinctions, while higher layers represent broader aggregations that reveal global semantic structural patterns. This hierarchical structure captures both local and global semantic relationships, enhancing the ability to distinguish subtle uncertainty differences. More illustration of the hierarchical abstraction is provided in Appendix VIII-B.

### C. SeSE for Long-form Generation

In practice, LLMs often generate long-form paragraphs containing multiple **claims** [27], which are the smallest semantically distinct units of information presented within the outputs. Therefore, in long-form generation, we assess uncertainty at the finer-grained claim level rather than assigning a single uncertainty score to an entire response or sentence. We have the following observation: given a context  $x$ , a set of randomly sampled responses  $\mathcal{R}$ , and a set of claims  $\mathcal{C}$  extracted from the greedily decoded response  $r_{T=0}$ , we can construct a bipartite graph  $G_{cr} = ((\mathcal{R}, \mathcal{C}), \mathcal{E})$  where the edge set  $\mathcal{E}$  represents semantic interactions between  $\mathcal{R}$  and  $\mathcal{C}$ . The graph  $G_{cr}$  thus captures semantic dependencies between responses  $\mathcal{R}$  and claims  $\mathcal{C}$ , from which we can extract information that reflects the uncertainty associated with each claim  $c \in \mathcal{C}$ . Intuitively, a claim that is densely connected to the response subgraph (i.e., consistently supported across sampled outputs) is more likely to be factually correct. Conversely, a sparsely connected claim is more likely to be a hallucination. As shown in Fig. 3, we first construct  $G_{cr} = ((\mathcal{R}, \mathcal{C}), \mathcal{E})$  and then estimate claim-level uncertainty using SeSE on this graph for hallucination detection. All prompt templates used in this process are provided in Appendix VIII-F.

1) *Response Sampling and Claim Decomposition:* Using the same sampling settings as in Section III-B1, we prompt LLMs to sample a stochastic response set  $\mathcal{R}(\cdot | x)$  and a greedily decoded response  $r_{T=0}$ . Then, we prompt GPT-5-mini with a specific template to decompose  $r_{T=0}$  into atomic claims, resulting in the claim set  $\mathcal{C}$ .

2) *Bipartite Graph Construction:* The bipartite graph  $G_{cr}$  is constructed by establishing connections between the response set  $\mathcal{R}$  and the claim set  $\mathcal{C}$ . An edge  $e \in \mathcal{E}$  is created between a response  $r \in \mathcal{R}$  and a claim  $c \in \mathcal{C}$  if  $r$  entails  $c$ . Edge weights are binary: 1 if entailment holds and 0 otherwise. We leverage the nuanced logical understanding of GPT-5-mini to assess entailment, thus avoiding the brittleness of manually tuned thresholds based on embedding distance or density-based clustering. The related ablation results for the entailment estimator are presented in Appendix VIII-D3.

3) *Claim-level Uncertainty Estimation:* In the bipartite graph  $G_{cr} = ((\mathcal{R}, \mathcal{C}), \mathcal{E})$ , we model semantic interactions as random walks between response and claim vertices, and quantify the uncertainty of these interactions using structural entropy. By minimizing the  $K$ -dimensional structural entropy of  $G_{cr}$ , we obtain its optimal encoding tree  $\mathcal{T}_{cr}^*$ , which captures the inherent hierarchical community structure over  $\mathcal{C}$  and  $\mathcal{R}$ . Following the same process in Section III-B3, we start by initializing a single-layer encoding tree  $\mathcal{T}_{cr}$  in which each leaf node  $\gamma$  has the tree root  $\lambda$  as its parent. Then, we obtain the

optimal  $K$ -dimensional encoding tree  $\mathcal{T}_{cr}^*$  using Algorithm 3. In  $\mathcal{T}_{cr}^*$ , the root node  $\lambda$  corresponds to the union of claim and response sets,  $\mathcal{T}_\lambda = \mathcal{R} \cup \mathcal{C}$ . Each leaf node  $\gamma$  is a singleton containing an individual claim or response, and intermediate nodes represent hierarchical abstractions at different levels.

The structural entropy associated with each non-root node  $\alpha$  quantifies the uncertainty of a random walk transitioning from the parent community  $\mathcal{T}_{\alpha^-}$  to its child community  $\mathcal{T}_\alpha$ . For any claim  $c \in \mathcal{C}$ , the uncertainty of reaching  $c$  is determined by the cumulative entropy of all nodes  $\alpha$  encountered along the path from the root node  $\lambda$  to the leaf node  $\gamma$  with  $V_\gamma = \{c\}$ . Accordingly, we define the SeSE of each claim  $c$  as its uncertainty of engaging in random semantic interactions within  $G_{cr}$  as detailed below:

$$SeSE(G_{cr}; c) = - \sum_{V_\gamma \subseteq V_\alpha \subset V} \frac{g_\alpha}{V_\lambda} \log_2 \frac{V_\alpha}{V_{\alpha^-}}. \quad (17)$$

Nodes with low SeSE typically reside in the network’s core regions, corresponding to claims that are frequently accessed during LLM generation, and are therefore more likely to be true. Conversely, claims with high SeSE often occupy peripheral or sparsely connected regions, indicating a high likelihood of being hallucinations.

#### IV. EXPERIMENTAL SETUP

This section details the experimental setup of our study. We introduce the datasets and LLMs used in our experiments in Section IV-A. Subsequently, we describe the comparison baselines in Section IV-B and present the evaluation metrics in Section IV-C.

##### A. Datasets and LLMs

1) *Datasets*: For sentence-length experiments, we employ five representative free-form QA datasets spanning diverse domains of natural language generation: BioASQ [37] (biomedical sciences), SVAMP [38] (mathematical word problems), TriviaQA [39] (trivia knowledge), NQ-Open [40] (open-domain natural questions from Google search queries), and SQuAD\_V2 [41] (commonsense knowledge). For long-form generation experiments, we evaluate on two challenging datasets featuring real-world entities from Wikipedia: FActScore [27] and PopQA [42]. To ensure data quality, we exclude entities with multiple Wikipedia entries or those with pages shorter than 2,000 tokens. For each dataset, we randomly sample 100 entities and generate a set of claims for each entity. This process yields over 1800 labeled claims (true or false) on average for each model-dataset combination. Further dataset details are provided in Appendix VIII-G.

2) *Studied LLMs*: We select the most advanced LLMs available at the time of writing. For sentence-length generation experiments, we use the Llama-3-Instruct series (3B, 8B, and 70B parameters) [43] and the Qwen-3-Instruct series (4B and 30B parameters) [44]. For long-form generation experiments, we involve DeepSeek-V3.1 [45] and close-sourced Gemini-2.5-Flash [46].

##### B. Baselines

We conduct a systematic comparison of SeSE against a range of strong baselines to validate its superiority. In

sentence-level experiments, we evaluate the following approaches: (1) Embedding Regression (ER) [24] extracts the final hidden states of LLMs and trains a classifier to predict answer correctness. (2) P(True) [24] uses few-shot prompting to guide LLMs in estimating the probability that their most confident answer is true. (3) SelfCheck-Prompt (SC-Prompt) is the prompt-based variant of SelfCheckGPT [25]. (4) Length-normalized Predictive Entropy (LN-PE) [47] computes the average token log-probability of generated sequences with length normalization. (5) Semantic Entropy (SE) [14], [16] estimates the entropy over semantic distributions of generated sequences. (6) Discrete Semantic Entropy (DSE) [16] is the black-box variant of semantic entropy. (7) Kernel Language Entropy (KLE) [17] is the generalization of semantic entropy using semantic kernels.

In the long-form generation experiments, we focus on the black-box scenario that more closely reflects real-world user applications. Besides variants of DSE, SC-Prompt, and P(True) which have been adapted to work for long-form generation, we also compare two verbalized confidence methods [22]: Post-hoc Verbalized Confidence (PH-VC) and In-line Verbalized Confidence (IL-VC), alongside a family of graph centrality metrics [19] including Betweenness, Eigenvalue, PageRank, and Closeness. Comprehensive details of all baseline methods are provided in Appendix VIII-H.

##### C. Evaluation Metrics

Following previous works, we assess two primary metrics. The first is the widely used Area Under the Receiver Operating Characteristic curve (AUROC), which measures classifier reliability by integrating precision and recall. AUROC values range from 0 to 1, where 1 denotes a perfect classifier and 0.5 indicates random classification. We also calculate the Area Under the Rejection Accuracy Curve (AURAC) [48], which quantifies the potential accuracy improvement users may experience when employing different UQ metrics to exclude high-uncertainty queries. X% rejection accuracy represents model performance on the subset of questions retained after filtering out top X% high-uncertainty queries, and AURAC provides a comprehensive assessment of accuracy across multiple rejection thresholds. Compared with AUROC, AURAC is more sensitive to changes in the overall accuracy of LLMs, and is particularly suitable for evaluating the UQ method’s ability to reduce erroneous responses.

We use GPT-5-mini to automatically evaluate the correctness of model-generated answers by comparing them with reference answers. This serves as the basis for calculating AUROC and AURAC. We manually check the quality of our automated ground-truth evaluation against human judgment, and the relevant results are shown in Appendix VIII-D2.

#### V. EXPERIMENTAL RESULTS

In this section, we conduct extensive experiments to demonstrate the effectiveness of our proposed SeSE. Through the experiments, we aim to answer the following four research questions: *RQ1* (Effectiveness): How effective is SeSE in detecting hallucinations in LLMs? *RQ2* (Generalization): How does SeSE perform on generation tasks across various domains? *RQ3* (Stability): How stable is SeSE in its hallucination

Table I: **RQ1**: Detailed experimental results of **25** model-dataset pairs in sentence-length generation.

Model/Method		BioASQ [37]		NQ-Open [40]		SQuAD [41]		SVAMP [38]		TriviaQA [39]		Avg./ $\Delta_{\uparrow}^{\%}$	
		AUROC	AURAC	AUROC	AURAC	AUROC	AURAC	AUROC	AURAC	AUROC	AURAC	AUROC	AURAC
Llama-3.2-3B	P(True) [24]	0.60±0.06	0.47±0.12	0.77±0.06	0.46±0.04	0.64±0.10	0.24±0.07	0.80±0.05	0.73±0.03	0.83±0.06	0.76±0.05	0.73	0.53
	ER [24]	0.63±0.03	0.51±0.10	0.62±0.03	0.38±0.04	0.61±0.04	0.22±0.04	0.63±0.05	0.60±0.03	0.70±0.03	0.62±0.02	0.64	0.46
	SC-Prompt [25]	0.72±0.04	0.56±0.08	0.77±0.04	0.46±0.03	0.73±0.04	0.28±0.07	0.75±0.02	0.72±0.02	0.87±0.01	0.78±0.02	0.77	0.56
	LN-PE [47]	0.69±0.04	0.52±0.08	0.74±0.03	0.43±0.03	0.75±0.02	0.29±0.07	0.68±0.02	0.65±0.02	0.81±0.01	0.75±0.01	0.73	0.53
	SE [16]	0.68±0.05	0.51±0.07	0.72±0.03	0.43±0.03	0.75±0.02	0.29±0.07	0.75±0.02	0.71±0.02	0.81±0.02	0.74±0.02	0.74 $\Delta_{\text{base}}$	0.53 $\Delta_{\text{base}}$
	DSE [16]	0.69±0.03	0.53±0.08	0.73±0.02	0.44±0.02	0.74±0.03	0.31±0.07	0.75±0.03	0.70±0.02	0.82±0.03	0.75±0.02	0.75+0.3%	0.55+2.0%
	KLE [17]	0.74±0.04	0.57±0.08	0.77±0.04	0.46±0.03	0.77±0.03	0.31±0.07	0.82±0.01	0.75±0.01	0.84±0.01	0.76±0.02	0.79+5.9%	0.57+6.4%
SeSE(Ours)	0.77±0.03	0.56±0.08	0.79±0.03	0.47±0.02	0.79±0.03	0.32±0.07	0.89±0.01	0.76±0.01	0.87±0.01	0.79±0.01	0.82+10.7%	0.58+8.5%	
Llama-3.1-8B	P(True) [24]	0.68±0.02	0.56±0.03	0.68±0.02	0.43±0.03	0.63±0.03	0.27±0.03	0.68±0.06	0.60±0.03	0.76±0.05	0.72±0.02	0.69	0.52
	ER [24]	0.67±0.03	0.57±0.02	0.64±0.03	0.41±0.03	0.59±0.02	0.24±0.04	0.72±0.02	0.62±0.01	0.71±0.01	0.66±0.01	0.66	0.50
	SC-Prompt [25]	0.66±0.03	0.55±0.02	0.69±0.02	0.44±0.02	0.63±0.03	0.26±0.03	0.78±0.03	0.65±0.02	0.72±0.02	0.68±0.01	0.70	0.52
	LN-PE [47]	0.64±0.02	0.54±0.02	0.66±0.03	0.41±0.03	0.66±0.02	0.28±0.05	0.55±0.02	0.49±0.01	0.66±0.03	0.66±0.02	0.63	0.48
	SE [16]	0.64±0.01	0.53±0.01	0.68±0.03	0.43±0.02	0.64±0.02	0.27±0.04	0.55±0.02	0.51±0.01	0.66±0.03	0.64±0.01	0.63 $\Delta_{\text{base}}$	0.48 $\Delta_{\text{base}}$
	DSE [16]	0.64±0.02	0.56±0.03	0.68±0.01	0.44±0.02	0.64±0.02	0.27±0.04	0.55±0.03	0.50±0.02	0.68±0.02	0.64±0.01	0.64+0.6%	0.49+2.7%
	KLE [17]	0.68±0.02	0.57±0.02	0.71±0.02	0.46±0.02	0.67±0.02	0.30±0.04	0.66±0.02	0.58±0.02	0.76±0.03	0.71±0.01	0.69+9.4%	0.52+10.2%
SeSE(Ours)	0.70±0.02	0.58±0.02	0.77±0.03	0.46±0.03	0.69±0.02	0.35±0.04	0.72±0.03	0.60±0.02	0.78±0.01	0.73±0.01	0.73+15.3%	0.54+14.4%	
Llama-3.1-70B	P(True) [24]	0.74±0.02	0.72±0.02	0.69±0.01	0.62±0.01	0.72±0.02	0.50±0.03	0.82±0.02	0.88±0.01	0.77±0.05	0.90±0.01	0.75	0.72
	ER [24]	0.73±0.03	0.74±0.03	0.64±0.02	0.59±0.02	0.63±0.03	0.51±0.04	0.73±0.04	0.83±0.02	0.66±0.03	0.88±0.01	0.68	0.71
	SC-Prompt [25]	0.75±0.02	0.72±0.02	0.69±0.03	0.62±0.03	0.81±0.03	0.56±0.04	0.86±0.02	0.90±0.01	0.81±0.04	0.91±0.01	0.78	0.74
	LN-PE [47]	0.74±0.02	0.72±0.03	0.70±0.03	0.63±0.02	0.70±0.02	0.48±0.04	0.73±0.03	0.86±0.01	0.74±0.02	0.90±0.01	0.72	0.72
	SE [16]	0.79±0.02	0.74±0.02	0.72±0.03	0.64±0.02	0.78±0.04	0.53±0.04	0.83±0.03	0.88±0.01	0.76±0.05	0.90±0.01	0.78 $\Delta_{\text{base}}$	0.74 $\Delta_{\text{base}}$
	DSE [16]	0.79±0.02	0.75±0.03	0.73±0.04	0.64±0.03	0.78±0.03	0.52±0.04	0.84±0.00	0.88±0.01	0.78±0.05	0.90±0.01	0.78+0.9%	0.74+0.6%
	KLE [17]	0.83±0.02	0.77±0.02	0.75±0.03	0.66±0.02	0.79±0.02	0.54±0.04	0.87±0.02	0.89±0.01	0.81±0.03	0.91±0.01	0.81+4.2%	0.75+2.2%
SeSE(Ours)	0.84±0.01	0.77±0.02	0.80±0.02	0.70±0.01	0.83±0.03	0.57±0.04	0.88±0.01	0.94±0.01	0.82±0.04	0.91±0.01	0.83+7.3%	0.78+5.4%	
Qwen-3-4B	P(True) [24]	0.75±0.02	0.67±0.03	0.80±0.08	0.44±0.02	0.75±0.04	0.39±0.06	0.85±0.01	0.84±0.01	0.83±0.05	0.74±0.02	0.79	0.61
	ER [24]	0.72±0.02	0.68±0.01	0.72±0.05	0.35±0.03	0.64±0.05	0.33±0.04	0.80±0.02	0.80±0.00	0.76±0.03	0.78±0.02	0.73	0.59
	SC-Prompt [25]	0.74±0.01	0.66±0.01	0.76±0.02	0.40±0.02	0.75±0.03	0.40±0.04	0.87±0.02	0.85±0.01	0.78±0.03	0.72±0.02	0.78	0.60
	LN-PE [47]	0.74±0.04	0.66±0.03	0.77±0.06	0.42±0.03	0.77±0.06	0.42±0.07	0.70±0.06	0.76±0.02	0.78±0.05	0.78±0.02	0.76	0.60
	SE [16]	0.73±0.03	0.65±0.01	0.79±0.04	0.43±0.02	0.77±0.03	0.41±0.04	0.70±0.01	0.77±0.01	0.82±0.04	0.73±0.02	0.76 $\Delta_{\text{base}}$	0.60 $\Delta_{\text{base}}$
	DSE [16]	0.74±0.03	0.65±0.03	0.79±0.04	0.42±0.02	0.77±0.01	0.41±0.03	0.70±0.02	0.77±0.01	0.84±0.03	0.74±0.02	0.77+0.5%	0.60+0.0%
	KLE [17]	0.78±0.02	0.67±0.02	0.80±0.03	0.43±0.02	0.79±0.03	0.40±0.04	0.79±0.02	0.81±0.01	0.85±0.04	0.75±0.02	0.80+5.4%	0.61+2.7%
SeSE(Ours)	0.79±0.02	0.68±0.01	0.81±0.02	0.44±0.02	0.80±0.02	0.42±0.04	0.87±0.02	0.86±0.01	0.87±0.04	0.78±0.01	0.83+8.5%	0.63+6.2%	
Qwen-3-30B-A3B	P(True) [24]	0.70±0.02	0.70±0.05	0.80±0.03	0.57±0.06	0.68±0.03	0.43±0.09	0.90±0.04	0.89±0.03	0.84±0.05	0.87±0.03	0.79	0.69
	ER [24]	0.76±0.03	0.70±0.03	0.67±0.01	0.54±0.06	0.64±0.02	0.48±0.08	0.85±0.02	0.84±0.02	0.73±0.05	0.83±0.03	0.73	0.68
	SC-Prompt [25]	0.74±0.01	0.71±0.05	0.77±0.02	0.54±0.05	0.68±0.02	0.42±0.10	0.89±0.03	0.89±0.03	0.86±0.05	0.87±0.03	0.79	0.69
	LN-PE [47]	0.70±0.03	0.70±0.05	0.75±0.01	0.53±0.06	0.69±0.03	0.43±0.09	0.68±0.02	0.82±0.02	0.68±0.05	0.81±0.03	0.70	0.66
	SE [16]	0.73±0.02	0.71±0.03	0.76±0.01	0.53±0.06	0.75±0.02	0.46±0.09	0.83±0.02	0.87±0.03	0.73±0.05	0.82±0.03	0.75 $\Delta_{\text{base}}$	0.68 $\Delta_{\text{base}}$
	DSE [16]	0.73±0.03	0.71±0.05	0.77±0.04	0.54±0.08	0.75±0.03	0.47±0.09	0.80±0.03	0.86±0.03	0.75±0.05	0.83±0.03	0.77+1.6%	0.68+1.0%
	KLE [17]	0.75±0.02	0.72±0.05	0.79±0.02	0.56±0.05	0.76±0.02	0.47±0.10	0.84±0.02	0.88±0.02	0.78±0.05	0.84±0.03	0.79+4.3%	0.69+2.4%
SeSE(Ours)	0.76±0.01	0.75±0.04	0.80±0.01	0.58±0.05	0.76±0.03	0.48±0.10	0.88±0.02	0.87±0.02	0.79±0.04	0.87±0.02	0.80+6.1%	0.71+5.0%	

The rounded results are the average of five experiments with various random seed. In each scenario, the best average results are **bolded**.

The Avg./ $\Delta_{\uparrow}^{\%}$  presents the LLM-wise percentage improvement of corresponding method compared to the based metric SE (SE).

detection performance? *RQ4* (Hyperparameter Sensitivity): How do the sampling numbers and encoding tree height impact SeSE’s overall performance? Furthermore, we conduct the ablation study in Section V-E and case study in Section V-F. The computational analysis is provided in Appendix VIII-C.

#### A. Effectiveness (RQ1)

1) *Detecting hallucinations in QA and math*: Table I summarizes the sentence-length experimental results across various datasets and LLMs. The results show that SeSE consistently outperforms strong baselines across different model families (Llama-3 and Qwen-3) and parameter scales (ranging from 3B to 70B). For example, with Llama-3.1-8B, SeSE achieves improvements of 15.3% in AUROC and 14.4% in AURAC compared with the base SE baseline. On average across the five LLMs, SeSE significantly surpasses all entropy-based baselines. Relative to KLE, a recent refinement of SE, SeSE achieves an average improvement of 3.5% in AUROC and 3.0% in AURAC. The LN-PE performs the worst, as it computes average predictive entropy solely from token-sequence probabilities, thereby conflating semantic and lexical uncertainty. Although KLE attempts to use the von Neumann graph entropy of semantic graph kernels to mitigate the one-cut semantic equivalence limitation of SE, it still performs semantic analysis at a single, non-hierarchical abstraction level. In contrast, SeSE constructs hierarchical semantic abstractions, enabling more precise modeling of uncertainty across multiple semantic levels. The substantial improvement in AURAC in-

dicates that SeSE provides finer discrimination of nuanced uncertainties. Moreover, SeSE also achieves better performance than advanced white-box methods without modifying LLMs’ internal architecture or introducing additional components.

2) *Detecting hallucinations in long-form generation*: We find that even the most advanced LLMs exhibit significant hallucination rates in our custom long-form datasets (including 7,407 claims), with 28% for DeepSeek-V3.1 and 27% for Gemini-2.5-Flash, on average. As shown in Table II, SeSE effectively identifies hallucinations in long-form generation with superior AUROC and AURAC scores compared to all baselines, including higher-cost methods such as SC-Prompt. For Gemini-2.5-Flash, SeSE delivers average improvements of 4.69% in AUROC and 2.07% in AURAC over the second-best DSE. We also observe that SeSE outperforms a range of graph centrality metrics, demonstrating its superior ability to identify central nodes within the claim-response graph. Additionally, verbalized confidence performs poorly, suggesting contemporary LLMs remain overconfident even when they should be uncertain about the factuality of their responses. Therefore, reliable uncertainty estimators are crucial for building user trust in LLMs and mitigating deployment risks in high-stakes scenarios.

#### B. Generalization (RQ2)

Figure 4a illustrates the hallucination rates of used LLMs on each dataset. As can be seen, our experiments cover a range of LLMs with varying hallucination levels across

Table II: **RQ1**: Detailed experimental results of 4 model-dataset pairs in long-form generation.

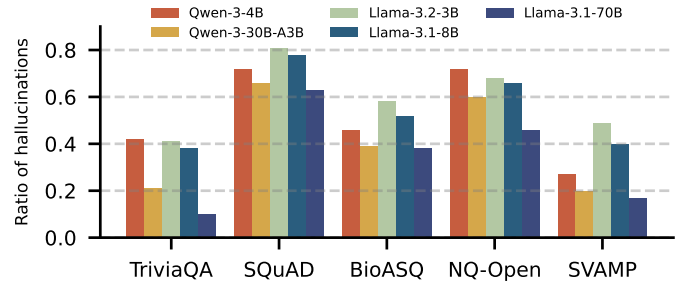
Model/Method	FactScore [27]		PopQA [42]		
	AUROC	AURAC	AUROC	AURAC	
DeepSeek-V3.1	DSE	0.7842	0.7684	0.7291	0.8094
	IL-VC	0.6838	0.7281	0.5820	0.7394
	PH-VC	0.7637	0.7606	0.6476	0.7813
	P(True)	0.7022	0.7371	0.6307	0.7709
	SC-Prompt	0.6066	0.6747	0.6210	0.7703
	Eigenvalue	0.6273	0.6759	0.5567	0.7165
	Betweenness	0.6495	0.7097	0.5926	0.7451
	PageRank	0.5701	0.6436	0.6033	0.7562
	Closeness	0.7598	0.7502	0.7147	0.8036
	<b>SeSE(Ours)</b>	<b>0.8105</b>	<b>0.7801</b>	<b>0.7468</b>	<b>0.8224</b>
<i>Abs.(%)</i> ↑	↑ <b>3.35%</b>	↑ <b>1.52%</b>	↑ <b>2.43%</b>	↑ <b>1.61%</b>	
Gemini-2.5-Flash	DSE	0.8504	0.8158	0.8348	0.8010
	IL-VC	0.5187	0.5960	0.5248	0.5395
	PH-VC	0.6397	0.6944	0.6483	0.6289
	P(True)	0.7204	0.7388	0.6427	0.6170
	SC-Prompt	0.7438	0.7529	0.8082	0.7904
	Eigenvalue	0.5697	0.6428	0.7210	0.7498
	Betweenness	0.6079	0.6772	0.7054	0.7371
	PageRank	0.6572	0.7026	0.7478	0.7764
	Closeness	0.7804	0.7912	0.7881	0.7805
	<b>SeSE(Ours)</b>	<b>0.8781</b>	<b>0.8286</b>	<b>0.8859</b>	<b>0.8216</b>
<i>Abs.(%)</i> ↑	↑ <b>3.26%</b>	↑ <b>1.57%</b>	↑ <b>6.12%</b>	↑ <b>2.57%</b>	

The best results are **bolded**, and the second-best results are underlined. *Abs.(%)* ↑ presents the percentage improvement of **bolded** method compared to underlined method.

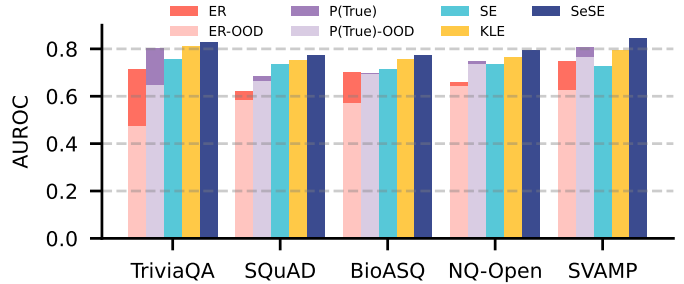
diverse generation tasks. The values plotted in Figure 4b represent the aggregate AUROC scores over five LLMs. Embedding regression is a representative supervised approach that utilizes a trained logistic regression classifier to predict answer correctness. P(True) serves as an “in-context” supervised method that adapts to specific tasks through few-shot demonstrations in the prompt. As indicated by the light red and light purple bars, both P(True) and ER suffer substantial performance degradation when the data distribution shifts between training and testing. In contrast, as an “off-the-shelf” unsupervised method, SeSE consistently outperforms both supervised and entropy-based baselines in in-distribution and out-of-distribution (OOD) datasets, demonstrating robust generalization capability and substantial practical utility. Such generalization is particularly important for UQ, as real-world scenarios often involve distribution shifts between training and deployment phases, and reliable UQ methods should perform well across diverse conditions.

### C. Stability (RQ3)

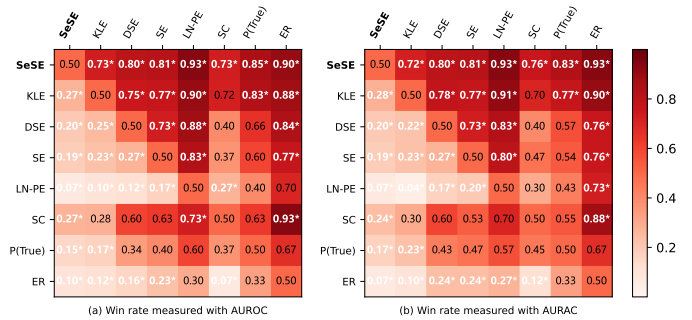
Results presented in the preceding chapters demonstrate that SeSE effectively detects hallucinations in the question-answering process of various LLMs and exhibits strong generalization across multiple domains. An additional crucial aspect is the stability of SeSE’s performance as a hallucination detector for LLMs. Given the inherent stochasticity of LLM generation [49], it is essential to evaluate whether SeSE’s performance is influenced by these uncertainties. To this end, we conduct five repeated experiments with distinct random seeds across 25 experimental scenarios (25 model-dataset pairs), resulting in a total of 125 runs. For each run, a 95% confidence interval is computed using 1,000 bootstrap resampling. While standard errors are reported in Table I, it should be noted that, in the context of LLM uncertainty quantification, standard errors tend to depend more on the LLM and dataset than on the UQ method itself. Rather



(a) Hallucination rate of LLMs across used datasets.



(b) Dataset-wise performance comparison. OOD represents the method is evaluated on out-of-distribution datasets.

Figure 4: **RQ2**: Hallucination rate of used LLMs in different domains and performance comparison in OOD datasets.Figure 5: **RQ3**: Pairwise win rates across 25 model-dataset scenarios. White value with asterisks (\*) indicates the binomial statistical significance level  $p < 0.05$  according.

than absolute values, the consistency of relative results across scenarios serves as a more reliable indicator of performance variation [16]. Therefore, we adopt the pairwise win rate as the primary evaluation metric and assess statistical significance using a binomial test. Within each scenario, the method with more wins across the five repeated trials is deemed superior. The heatmaps in Figure 5 visualize the pairwise win rates, showing that SeSE consistently outperforms baselines at a significance level of  $p < 0.05$ . This finding indicates that, although SeSE’s performance may vary across scenarios, its comparative advantage remains highly consistent, making it a more stable uncertainty estimator in practical applications.

### D. Sensitivity to Hyperparameters (RQ4)

1) *Sensitivity to Sampling Numbers*: The number of sampled responses  $N$  does not need to be large. Figure 6a illustrates how the hallucination detection performance varies with  $N$  for sentence-length generations, while Figure 6b presents the corresponding results for long-form generations. The reported values are aggregated across all datasets and LLMs. For sentence-length generations, performance gains show diminishing returns at  $N \approx 5$ . However, increasing  $N$  to 10 can still be beneficial. For long-form generation, we find

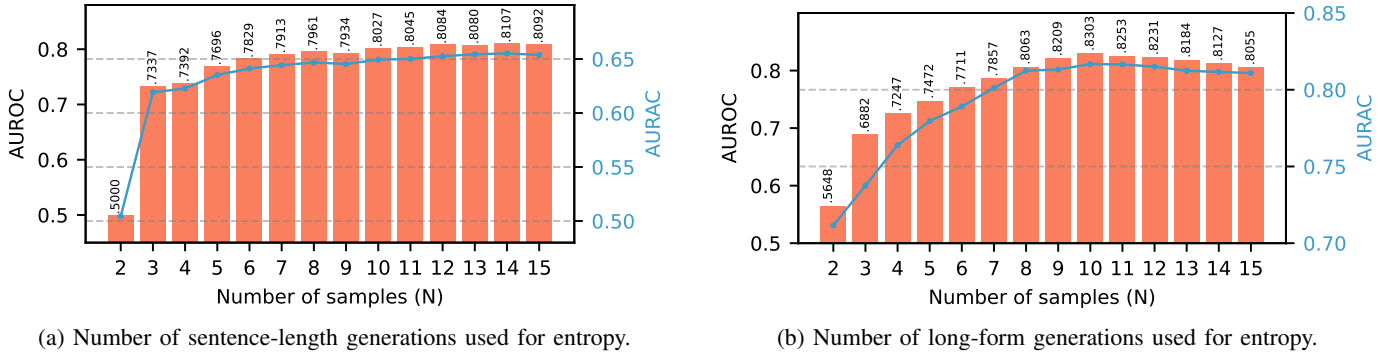


Figure 6: **RQ4.1:** The performance of SeSE with different number of sampled responses ( $N$ ).

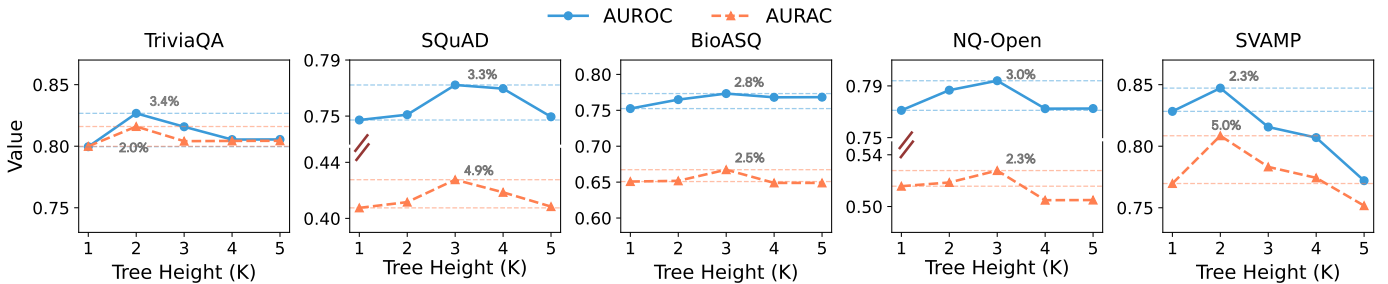


Figure 7: **RQ4.2:** The performance of SeSE when adopting different tree height  $K$ .

that optimal performance is achieved with 9–10 responses. Different from sentence-level generation, more generations don’t always improve performance. This occurs because the stochastic decoding strategies are commonly employed to boost the output diversity of LLMs [49], which increases the likelihood of selecting low-probability tokens. Excessively increasing sample numbers amplifies the selection probability of low-probability tokens, potentially introducing irrelevant content and thereby diminishing the relative weight of original claims from greedy decoding. In this study, we set  $N = 10$  for both sentence-length and long-form experiments.

2) *Sensitivity to Encoding Tree Height:* Figure 7 shows SeSE’s performance sensitivity to encoding tree height  $K$ . The accuracy improvement of the best tree height compared with  $K = 1$  is annotated in the figure. When  $K = 1$ , SeSE degenerates to the non-hierarchical von Neumann graph entropy [31]. Compared with  $K = 1$ , SeSE achieves optimal performance on two and three datasets at  $K = 2$  and  $K = 3$ , respectively. We also observe that the optimal  $K$  correlates with task difficulty. For instance, on the simpler dataset TriviaQA, SeSE peaks at  $K = 2$ , while on the challenging SQuAD, the optimum is found at  $K = 3$ . These findings demonstrate that SeSE can flexibly adapt to diverse downstream tasks with optional encoding tree depth. We provide unaggregated results for Figure 6 and additional statistics with detailed analyses for Figure 7 in Appendix VIII-D4.

### E. Ablation Study

Table III presents the ablation study on hallucination detection performance under different graph uncertainty metrics and semantic graph construction schemes. Specifically, in the experiments on graph uncertainty metrics, only the structural entropy is replaced with alternative metrics, including Eigenvalue, Eccentricity, Spectral Gap and Degree [19]. SeSE-undir denotes the use of an undirected semantic graph, and SeSE-com refers to a complete semantic graph. Among all

variants, the complete SeSE achieves the best results across all experimental settings. First, SeSE outperforms all other graph uncertainty metrics. They essentially simplify the graph into a collection of nodes and edges with specific probabilistic distributions, overlooking critical semantic topological structures that convey the core graph information. In contrast, SeSE formalizes hierarchical abstraction through an encoding tree, effectively capturing the semantic structural information. Second, removing either directed semantic modeling or graph sparsification results in a decline in detection performance. As shown in Figure 8, the undirected complete graph (see (a)) contains numerous edges with near-zero weights and obfuscate the asymmetric nature of semantic spaces (see (b)). Only the “dir” + “sparsification” combination (see (c)) optimally models the semantic space, effectively revealing both core semantic distributions and directional relationships. Detailed definitions of the used graph uncertainty metrics are provided in Appendix Table VIII.

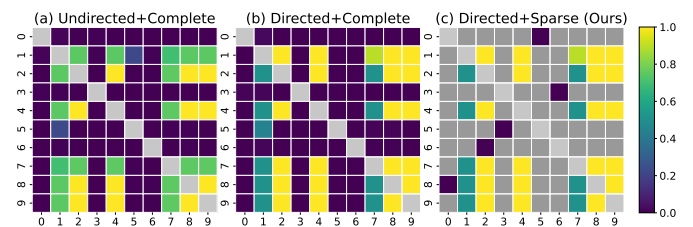


Figure 8: The adjacent matrix of the semantic space with different graph modeling methods. A gray grid represents that there is no edge between response  $i$  and  $j$ .

### F. Case Study

We present two representative examples from the SQuAD dataset in Figure 9. To analyze cases where SE and SeSE are inconsistent, we ranked all cases by SE and selected two examples with similar indices but different factual labels (Hallu/Non-hallu). As shown in Figure 9(a), when semantic

Table III: Ablation study of SeSE under different setups.

	Llama-3.2-3B		Llama-3.1-8B		Llama-3.1-70B		Qwen-3-4B		Qwen-3-30B	
	AUROC	AURAC								
Eccentricity	0.6664	0.5059	0.6305	0.4989	0.7259	0.7343	0.6919	0.5707	0.6773	0.6547
Spectral Gap	0.7187	0.5445	0.6530	0.5173	0.7705	0.7549	0.7546	0.6090	0.7479	0.6924
Eigenvalue	0.7833	0.5670	0.7007	0.5314	0.8027	0.7675	0.7913	0.6216	0.7785	0.6992
Degree	0.8117	0.5665	0.7247	0.5342	0.8211	0.7639	0.7979	0.6286	0.7953	0.6892
SeSE	<b>0.8145</b>	<b>0.5783</b>	<b>0.7356</b>	<b>0.5495</b>	<b>0.8330</b>	<b>0.7775</b>	<b>0.8266</b>	<b>0.6349</b>	<b>0.7992</b>	<b>0.7103</b>
SeSE-undir	0.7711	0.5585	0.7067	0.5250	0.8069	0.7514	0.7925	0.6127	0.7720	0.6872
SeSE-comple	0.7193	0.5220	0.6946	0.5177	0.7462	0.7110	0.7855	0.6098	0.7641	0.6841

The best results are **bolded**.

structures are ignored, the semantic spaces of these two cases appear superficially similar, both divisible into five semantic clusters with similar sizes. However, since SE solely estimates the Shannon entropy of semantic cluster probability distributions, it underestimates the divergence between these two cases, yielding a value of only 0.14. In contrast, SeSE employs an optimal  $K$ -dimensional encoding tree  $\mathcal{T}^*$  constructed according to the principle of structural information minimization, which captures the intrinsic hierarchical organization of the semantic space, i.e., compressing it most succinctly. The structural entropy of  $\mathcal{T}^*$  quantifies the minimal number of bits required to describe the semantic space [31]. As illustrated in Figures 9(a)–(c), increasing the depth of the encoding tree reveals that the hallucination case exhibits greater resistance to compression due to its disordered semantic structure, resulting in a final compression ratio of only 36%. Conversely, the non-hallucinated case, characterized by more regular semantic organization, is more readily compressed, achieving a final ratio of 46%. This difference increases the entropy gap  $\Delta_{SeSE}$  from 0.25 to 0.45. Consequently, SeSE effectively identifies fine-grained uncertainty distinctions even when existing semantic UQ methods fail [16], [17], [19]. Detailed information of the used cases is provided in Appendix VIII-E.

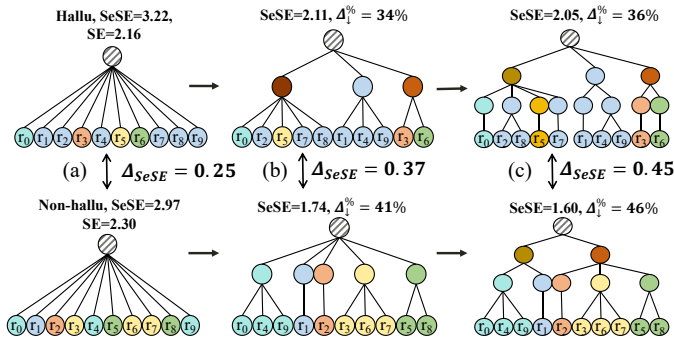


Figure 9: Two cases in which SeSE effectively identifies subtle uncertainty when SE fails.  $\Delta_{SeSE}$  represents the SeSE difference between the encoding tree of the 1<sup>st</sup> and 2<sup>nd</sup> row.  $\Delta_{\downarrow}^{\%}$  represents the compression ratio compared to the 1-dimensional encoding tree (i.e., part (a)).

## VI. RELATED WORK

### A. Uncertainty Estimation in LLMs

This section reviews the fundamental ideas of existing UQ methods and their potential limitations, which are then addressed in the development of SeSE.

The first direction is to conduct supervised learning, either by fine-tuning the base LLMs or by adding additional layers to obtain uncertainty scores [50], [51]. Despite their promise, as

these methods are often model-specific and require additional training, they have poor generalization ability and cannot be applied to closed-source models. In contrast, SeSE offers an “off-the-shelf” solution applicable across both open- and closed-source models without requiring any architectural modifications or additional training. The second line of research seeks to prompt LLMs to express their uncertainty about their own responses using natural language [22], [24], [52]. However, as noted by Kalai et al. [53], since most existing evaluation methods fail to incentivize models to express uncertainty honestly, LLMs tend to exhibit high confidence even when they might provide incorrect outputs. Overall, the performance of verbalized confidence is generally inferior to other more advanced methods [22].

The aforementioned methods primarily focus on token-level uncertainty, neglecting the model’s semantic uncertainty. In fact, semantic uncertainty is crucial for analyzing the hallucinations in LLM outputs, as it directly influences the accuracy of the models’ outputs. As a third direction, semantic entropy [14]–[16] is one of the most advanced metrics for quantifying uncertainty in the semantic space. It groups responses into semantic clusters and calculates the Shannon entropy of the resulting cluster probability distribution as the uncertainty metric. Although its performance generally surpasses that of other token-based approaches, it considers only the one-cut semantic equivalence relationship. Subsequent works like kernel language entropy [17] tried to address this issue using semantic graph kernels, but still suffer from two inherent limitations: (1) the adopted kernel functions make it challenging to interpret the model’s uncertainty; (2) semantic analysis is conducted at the same level without hierarchy, which violates the principle of “compositional similarity” and limits the ability to distinguish between fine-grained uncertainties. Based on structural information theory, our proposed SeSE enables fine-grained semantic analysis through the hierarchical encoding tree, thereby providing more precise uncertainty estimates.

### B. Structural Entropy

Structural entropy, originally introduced by Li and Pan [29], serves as a metric for graph uncertainty. It generalizes Shannon entropy from unstructured probability distributions to graphs with arbitrary topologies. Structural information theory employs an encoding tree to encode graphs, and minimizing structural entropy can reveal the intrinsic structure of graphs. In recent years, it has been widely employed in diverse domains, including graph kernels [54], text classification [32], social detection [55], and semi-supervised clustering [56]. However, most existing research on structural information focuses on undirected graphs, which fail to capture the irreversible logical

directional relationships between responses, leading to inevitable information loss. In this study, we optimize the native structural entropy for directed graphs to facilitate hierarchical abstracting under asymmetric scenarios.

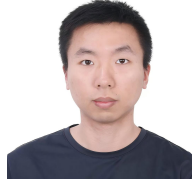
## VII. CONCLUSION

This paper proposes SeSE, a principled UQ framework based on structural information theory, capturing semantic structural information within semantic spaces to provide more precise uncertainty estimates. First, we develop an adaptively sparsified directed semantic graph construction algorithm to effectively model semantic spaces. Then, we perform hierarchical abstraction using an encoding tree to quantify the inherent semantic uncertainty of LLMs. Additionally, we extend SeSE to quantify claim-level uncertainty in long-form outputs, providing interpretable uncertainty estimates. SeSE outperforms existing competitors and is verified to be a reliable UQ framework for LLM hallucination detection. Notably, SeSE is an “off-the-shell”, opening up new possibilities for reliably deploying LLMs in resource-constrained environments.

## REFERENCES

- [1] C. Liu, K. H. Hettige, Q. Xu, C. Long, S. Xiang, G. Cong, Z. Li, and R. Zhao, “St-llm+: Graph enhanced spatio-temporal large language models for traffic prediction,” *IEEE Trans. Knowl. Data Eng.*, vol. 37, no. 8, pp. 4846–4859, 2025.
- [2] W. Lai, H. Xie, G. Xu, and Q. Li, “Multi-task learning with llms for implicit sentiment analysis: Data-level and task-level automatic weight learning,” *IEEE Trans. Knowl. Data Eng.*, pp. 1–12, 2025.
- [3] C. Zhao, X. Su, M. He, H. Zhao *et al.*, “Collaborative knowledge fusion: A novel method for multi-task recommender systems via llms,” *IEEE Trans. Knowl. Data Eng.*, vol. 37, no. 9, pp. 5017–5033, 2025.
- [4] O. Ovcharenko and X. Lian, “Cafe: Towards compact, adaptive, and fast embedding for large-scale recommendation models,” in *Proc. ACM SIGMOD Int. Conf. Manage. Data*, 2025, pp. 66 – 68.
- [5] Z. Zhao, W. Fan, J. Li *et al.*, “Recommender systems in the era of large language models (llms),” *IEEE Trans. Knowl. Data Eng.*, vol. 36, no. 11, pp. 6889–6907, 2024.
- [6] A. Liu, Q. Sheng, and X. Hu, “Preventing and detecting misinformation generated by large language models,” in *Proc. 47th Annu. Int. ACM SIGIR Conf. Res. Develop. Inf. Retrieval*, 2024, p. 3001–3004.
- [7] S. Pan, L. Luo, Y. Wang, C. Chen, J. Wang, and X. Wu, “Unifying large language models and knowledge graphs: A roadmap,” *IEEE Trans. Knowl. Data Eng.*, vol. 36, no. 7, pp. 3580–3599, 2024.
- [8] L. Yang, H. Chen, Z. Li, X. Ding, and X. Wu, “Give us the facts: Enhancing large language models with knowledge graphs for fact-aware language modeling,” *IEEE Trans. Knowl. Data Eng.*, vol. 36, no. 7, pp. 3091–3110, 2024.
- [9] J. J. Ross, E. Khramtsova, A. van der Vegt, B. Koopman, and G. Zuccon, “Rarr unraveled: Component-level insights into hallucination detection and mitigation,” in *Proc. 48th Annu. Int. ACM SIGIR Conf. Res. Develop. Inf. Retrieval*, 2025, p. 3286–3295.
- [10] E. Vakaj, N. Mihindukulasooriya, M. Gaur, and A. Khan, “Knowledge graphs for responsible ai,” in *Int Conf Inf Knowledge Manage*, 2024, p. 5596–5598.
- [11] X. Liu, T. Chen, L. Da, C. Chen, Z. Lin, and H. Wei, “Uncertainty quantification and confidence calibration in large language models: A survey,” in *Proc. 31th ACM SIGKDD Conf. Knowl. Discov. Data Mining*, 2025, pp. 6107–6117.
- [12] Y. Liu, W. Tao, T. Xia, S. Knight, and T. Zhu, “Survunc: A meta-model based uncertainty quantification framework for survival analysis,” in *Proc. 31th ACM SIGKDD Conf. Knowl. Discov. Data Mining*, 2025.
- [13] L. Kong, H. Kamarthi, P. Chen, B. A. Prakash, and C. Zhang, “Uncertainty quantification in deep learning,” in *Proc. 29th ACM SIGKDD Conf. Knowl. Discov. Data Mining*, 2023, p. 5809–5810.
- [14] L. Kuhn, Y. Gal, and S. Farquhar, “Semantic uncertainty: Linguistic invariances for uncertainty estimation in natural language generation,” in *Proc. Int. Conf. Learn. Representations*, 2023.
- [15] J. Han, J. Kossen, M. Razzak, L. Schut, S. A. Malik, and Y. Gal, “Semantic entropy probes: Robust and cheap hallucination detection in llms,” in *Proc. Int. Conf. Mach. Learn.*, 2024.
- [16] S. Farquhar, J. Kossen, L. Kuhn, and Y. Gal, “Detecting hallucinations in large language models using semantic entropy,” *Nature*, vol. 630, no. 8017, pp. 625–630, 2024.
- [17] A. Nikitin, J. Kossen, Y. Gal, and P. Marttinen, “Kernel language entropy: Fine-grained uncertainty quantification for llms from semantic similarities,” in *Adv. Neural Inf. Process. Syst.*, vol. 37, 2024, pp. 8901–8929.
- [18] O. Boiman and M. Irani, “Similarity by composition,” in *Adv. Neural Inf. Process. Syst.*, 2006, pp. 177–184.
- [19] Z. Lin, S. Trivedi, and J. Sun, “Generating with confidence: Uncertainty quantification for black-box large language models,” *Trans. Mach. Learn. Res.*, 2024.
- [20] L. Kotlerman, I. Dagan, I. Szpektor, and M. Zhitomirsky-Geffet, “Directional distributional similarity for lexical inference,” *Nat. Lang. Eng.*, vol. 16, no. 4, pp. 359–389, 2010.
- [21] Y. A. Yadkori, I. Kuzborskij, D. Stutz, A. György, A. Fisch, A. Doucet, I. Beloshapka, W.-H. Weng, Y.-Y. Yang, C. Szepesvári *et al.*, “Mitigating llm hallucinations via conformal abstention,” *arXiv:2405.01563*, 2024.
- [22] C. Mohri and T. Hashimoto, “Language models with conformal factuality guarantees,” in *Proc. Int. Conf. Mach. Learn.*, 2024, pp. 36029–36047.
- [23] V. Quach, A. Fisch, T. Schuster, A. Yala, J. H. Sohn, T. S. Jaakkola, and R. Barzilay, “Conformal language modeling,” in *Proc. Int. Conf. Learn. Representations*, 2024.
- [24] S. Kadavath, T. Conerly, A. Askell, Henighan *et al.*, “Language models (mostly) know what they know,” *arXiv:2207.05221*, 2022.
- [25] P. Manakul, A. Liusie, and M. J. Gales, “Selfcheckgpt: Zero-resource black-box hallucination detection for generative large language models,” in *Proc. Conf. Empir. Methods Natural Lang. Process.*, 2023.
- [26] X. Wang, J. Wei, D. Schuurmans, Q. V. Le, E. H. Chi, S. Narang, A. Chowdhery, and D. Zhou, “Self-consistency improves chain of thought reasoning in language models,” in *Proc. Int. Conf. Learn. Representations*, 2023.
- [27] S. Min, K. Krishna, X. Lyu, M. Lewis, W.-t. Yih, P. Koh, M. Iyyer, L. Zettlemoyer, and H. Hajishirzi, “Factscore: Fine-grained atomic evaluation of factual precision in long form text generation,” in *Proc. Conf. Empir. Methods Natural Lang. Process.*, 2023, pp. 12076–12100.
- [28] A. Li, X. Yin, and Y. Pan, “Three-dimensional gene map of cancer cell types: Structural entropy minimisation principle for defining tumour subtypes,” *Sci Rep*, vol. 6, no. 1, p. 20412, 2016.
- [29] A. Li and Y. Pan, “Structural information and dynamical complexity of networks,” *IEEE Trans. Inf. Theory*, vol. 62, no. 6, pp. 3290–3339, 2016.
- [30] M. Jiang, Y. Ruan, P. Sattigeri, S. Roukos, and T. B. Hashimoto, “Graph-based uncertainty metrics for long-form language model generations,” in *Adv. Neural Inf. Process. Syst.*, vol. 37, 2024, pp. 32980–33006.
- [31] A. Li, *Science of Artificial Intelligence: Mathematical Principles of Intelligence (In Chinese)*. Science Press, 2024.
- [32] Q. Liu, H. Peng, X. Huang, Z. Hao, Q. Sun, Z. Yu, and P. S. Yu, “Hierarchical text classification optimization via structural entropy and singular smoothing,” *IEEE Trans. Knowl. Data Eng.*, vol. 37, no. 9, pp. 5283 – 5297, 2025.
- [33] X. Zeng, H. Peng, and A. Li, “Effective exploration based on the structural information principles,” in *Adv. Neural Inf. Process. Syst.*, vol. 37, 2024, pp. 95291–95325.
- [34] R. Tarjan, “Depth-first search and linear graph algorithms,” *SIAM J. Comput.*, vol. 1, no. 2, pp. 146–160, 1972.
- [35] A. Holtzman, J. Buys, L. Du *et al.*, “The curious case of neural text degeneration,” in *Proc. Int. Conf. Learn. Representations*, 2020.
- [36] A. Fan, M. Lewis, and Y. Dauphin, “Hierarchical neural story generation,” in *Proc. Annu. Meet. Assoc. Comput. Linguist.*, vol. 1, 2018.
- [37] A. Krithara, A. Nentidis, K. Bougiatiotis, and G. Paliouras, “Bioasqqa: A manually curated corpus for biomedical question answering,” *Sci. Data*, vol. 10, no. 1, p. 170, 2023.
- [38] A. Patel, S. Bhattamishra, and N. Goyal, “Are nlp models really able to solve simple math word problems?” in *Proc. Conf. North American Chapter Assoc. Comput. Linguist.*, 2021, pp. 2080–2094.
- [39] M. Joshi, E. Choi, D. Weld, and L. Zettlemoyer, “Triviaqa: A large scale distantly supervised challenge dataset for reading comprehension,” in *Proc. Annu. Meet. Assoc. Comput. Linguist.*, vol. 1, 2017.
- [40] T. Kwiatkowski, J. Palomaki, O. Redfield *et al.*, “Natural questions: A benchmark for question answering research,” *Proc. Annu. Meet. Assoc. Comput. Linguist.*, vol. 7, pp. 453–466, 2019.
- [41] P. Rajpurkar, “Know what you don’t know: Unanswerable questions for squad,” in *Proc. Annu. Meet. Assoc. Comput. Linguist.*, vol. 2, 2018, pp. 784–789.

- [42] A. Mallen, A. Asai, V. Zhong, R. Das, D. Khashabi, and H. Hajishirzi, “When not to trust language models: Investigating effectiveness of parametric and non-parametric memories,” in *Proc. Annu. Meet. Assoc. Comput. Linguist.*, 2023, pp. 9802–9822.
- [43] Meta, “The llama 3 herd of models,” *arXiv:2407.21783*, 2024.
- [44] Qwen, “Qwen3 technical report,” *arXiv:2505.09388*, 2025.
- [45] DeepSeek-AI, “Deepseek-v3.1,” 2025. [Online]. Available: <https://hf-mirror.com/deepseek-ai/DeepSeek-V3.1-Terminus>
- [46] Google, “Gemini 2.5: Pushing the frontier with advanced reasoning, multimodality, long context, and next generation agentic capabilities,” *arXiv:2507.06261*, 2025.
- [47] A. Malinin and M. Gales, “Uncertainty estimation in autoregressive structured prediction,” in *Proc. Int. Conf. Learn. Representations*, 2021.
- [48] M. S. A. Nadeem, J.-D. Zucker, and B. Hanczar, “Accuracy-rejection curves (arcs) for comparing classification methods with a reject option,” in *Mach. Learn. Syst. Biol.*, 2009, pp. 65–81.
- [49] L. Huang, W. Yu, W. Ma, W. Zhong, Feng *et al.*, “A survey on hallucination in large language models: Principles, taxonomy, challenges, and open questions,” *ACM Trans. Inf. Syst.*, vol. 43, no. 2, pp. 1–55, 2025.
- [50] S. Liu, Z. Li, X. Liu, R. Zhan, D. Wong, L. Chao, and M. Zhang, “Can llms learn uncertainty on their own? expressing uncertainty effectively in a self-training manner,” in *Proc. Conf. Empir. Methods Natural Lang. Process.*, 2024, pp. 21 635–21 645.
- [51] J. Xie, A. Chen, Y. Lee, E. Mitchell, and C. Finn, “Calibrating language models with adaptive temperature scaling,” in *Proc. Conf. Empir. Methods Natural Lang. Process.*, 2024, pp. 18 128–18 138.
- [52] K. Tian, E. Mitchell, A. Zhou, A. Sharma *et al.*, “Just ask for calibration: Strategies for eliciting calibrated confidence scores from language models fine-tuned with human feedback,” *Proc. Conf. Empir. Methods Natural Lang. Process.*, pp. 5433 – 5442, 2023.
- [53] A. T. Kalai, O. Nachum, S. S. Vempala, and E. Zhang, “Why language models hallucinate,” *arXiv:2509.04664*, 2025.
- [54] R. Yang, H. Peng, A. Li, P. Li, C. Liu, and P. S. Yu, “Hierarchical abstracting graph kernel,” *IEEE Trans. Knowl. Data Eng.*, vol. 37, no. 2, pp. 724 – 738, 2025.
- [55] Y. Yang, Q. Wu, B. He *et al.*, “Sebot: Structural entropy guided multi-view contrastive learning for social bot detection,” in *Proc. ACM SIGKDD Int. Conf. Knowl. Discov. Data Min.*, 2024, pp. 3841–3852.
- [56] G. Zeng, H. Peng, A. Li, J. Wu, C. Liu, and P. S. Yu, “Scalable semi-supervised clustering via structural entropy with different constraints,” *IEEE Trans. Knowl. Data Eng.*, vol. 37, no. 1, pp. 478–492, 2025.



**Dingli Su** is a Ph.D. candidate in Software Engineering at Beihang University. His research focuses on building principled and collaborative multi-agent systems by combining structural information theory with reinforcement learning and large language models.



**Xianghua Zeng** is currently a Ph.D. candidate in the School of Computer Science and Engineering at Beihang University. His research interests include Reinforcement Learning and Structural Information Principle.



**Chunyang Liu** is currently a researcher with Didi Chuxing Technology Company, Ltd. His research interests include machine learning and structural data mining.



**Xingtao Zhao** is currently a Master's Degree candidate in the School of Cyber Science and Technology at Beihang University. His research interests include machine learning and deep learning.

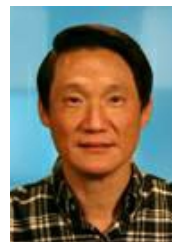


**Jinzhi Liao** obtained his Ph.D. from National University of Defense Technology and is currently an Associate Professor. His research interests include large language model and knowledge graph.



**Hao Peng** is currently a Professor at the School of Cyber Science and Technology at Beihang University. His research interests include representation learning, social network mining, and reinforcement learning. To date, Dr Peng has published over 150 research papers in top-tier journals and conferences, including the IEEE TKDE, TPAMI, TC, ACM TOIS, SIGIR, SIGKDD, ICML, NeurIPS. He is the Associate Editor of the IEEE/ACM Transactions on Audio, Speech, and Language Processing (TASLP), International Journal of Machine Learning and Cy-

bernetics (IJMLC), and Neural Networks.



**Philip S. Yu** is a Distinguished Professor and the Wexler Chair in Information Technology at the Department of Computer Science, University of Illinois at Chicago. Before joining UIC, he was at the IBM Watson Research Center, where he built a world-renowned data mining and database department. He is a Fellow of the ACM and IEEE. Dr. Yu was the Editor-in-Chief of ACM Transactions on Knowledge Discovery from Data (2011-2017) and IEEE Transactions on Knowledge and Data Engineering (2001-2004).

## APPENDIX

## A. Theoretical Proofs

In this section, we prove proposed Theorem 1 using the Perron-Frobenius theorem.

**Lemma 1** (Perron–Frobenius Theorem). *Let  $M \in \mathbb{R}^{n \times n}$  be an irreducible non-negative matrix. Then:*

- (1)  $\rho(M) = \max\{|\lambda| : \lambda \in \sigma(M)\}$  is an eigenvalue of  $M$ ;
- (2) There exists a positive vector  $\mathbf{x} > 0$  such that  $M\mathbf{x} = \rho(M)\mathbf{x}$ ;
- (3) The algebraic multiplicity of  $\rho(M)$  is 1;
- (4)  $M^\top$  is also irreducible and non-negative.

Given that  $A$  is a stochastic matrix, all its row sums equal 1. Hence, the all-ones vector  $\mathbf{e} = (1, 1, \dots, 1)^\top$  satisfies

$$A\mathbf{e} = \mathbf{e}, \quad (18)$$

which implies that 1 is an eigenvalue of  $A$ , i.e.,  $1 \in \sigma(A)$ . Therefore, the spectral radius  $\rho(A) = \max\{|\lambda| : \lambda \in \sigma(A)\}$  satisfies

$$\rho(A) \geq 1. \quad (19)$$

For any matrix  $M$ , the spectral radius is bounded above by its  $\infty$ -norm:  $\rho(M) \leq \|M\|_\infty$ , where  $\|M\|_\infty = \max_i \sum_j |M_{ij}|$ . Since  $A$  is stochastic, we have  $\|A\|_\infty = \max_i \sum_j A_{ij} = 1$ , and thus

$$\rho(A) \leq 1. \quad (20)$$

Combining both inequalities yields  $\rho(A) = 1$ .

A stationary distribution  $\pi^\top$  is defined by the condition  $\pi^\top A = \pi^\top$ , which is equivalent to

$$A^\top \pi = \pi. \quad (21)$$

Because  $A$  is irreducible and non-negative, its transpose  $A^\top$  is also irreducible and non-negative. Applying the Perron–Frobenius Theorem to  $A^\top$ , we conclude:

- The spectral radius  $\rho(A^\top) = 1$  is an eigenvalue of  $A^\top$ ;
- There exists a strictly positive eigenvector  $\pi > \mathbf{0}$  such that  $A^\top \pi = \pi$ ;
- The eigenvalue 1 has algebraic multiplicity one, so  $\pi$  is unique up to scalar multiplication.

We now normalize  $\pi$  by its  $\ell_1$ -norm:

$$\hat{\pi} = \frac{\pi}{\pi^\top \mathbf{e}}, \quad (22)$$

where  $\pi^\top \mathbf{e} = \sum_i \pi_i > 0$  since  $\pi > \mathbf{0}$ . By construction,  $\hat{\pi}^\top \mathbf{e} = \frac{\pi^\top \mathbf{e}}{\pi^\top \mathbf{e}} = 1$ , and

$$\hat{\pi}^\top A = \left( \frac{\pi}{\pi^\top \mathbf{e}} \right)^\top A = \frac{\pi^\top A}{\pi^\top \mathbf{e}} = \frac{\pi^\top}{\pi^\top \mathbf{e}} = \hat{\pi}^\top.$$

Hence,  $\hat{\pi}^\top$  is a stationary distribution.

To prove uniqueness, suppose  $\sigma^\top$  is another stationary distribution, i.e.,  $\sigma^\top A = \sigma^\top$ , which implies  $A^\top \sigma = \sigma$ . Then  $\sigma$  is a positive eigenvector of  $A^\top$  corresponding to the eigenvalue 1. Since the eigenspace is one-dimensional,  $\sigma$  must be a scalar multiple of  $\pi$ . After normalization, we obtain  $\sigma = \hat{\pi}$ , confirming the uniqueness of  $\hat{\pi}$ .

Therefore,  $G_{\text{dir}}$  admits a unique stationary distribution  $\hat{\pi}^\top$ , which is the unique normalized eigenvector of  $A^\top$  corresponding to the dominant eigenvalue 1.  $\square$

## B. Hierarchical Abstracting

Figure 10 illustrates the construction of a 2-dimensional hierarchical abstraction. Specifically, consider a semantic space represented by an irreducible non-negative matrix  $A_{n \times n}$ . Let  $V = \{1, 2, \dots, n\}$ , and let  $\mathcal{T}$  be an encoding tree for  $A$ . Assume  $\alpha$  and  $\beta$  are two leaf nodes in  $\mathcal{T}$  that share a common parent node  $\gamma$ , i.e.,  $\alpha^- = \beta^- = \gamma$ . The steps for adjusting the encoding tree using the merging operator of leaf nodes  $\alpha$  and  $\beta$  are as follows [31]:

- (1) Create a new node  $\delta = \gamma^{(i)}$ , and renumber the child nodes of  $\gamma$  as  $0, 1, \dots, k$ ;
- (2) Set  $T_\delta = \{x, y\}$ ;
- (3) Create two new nodes  $\delta^{(0)}, \delta^{(1)}$ ;
- (4) Define  $T_{\delta^{(0)}} = \{x\}$  and  $T_{\delta^{(1)}} = \{y\}$ ;
- (5) Delete  $\alpha$  and  $\beta$ .

Assume  $\alpha$  and  $\beta$  are two arbitrary nodes in  $\mathcal{T}$  that share a common parent node  $\gamma$ , i.e.,  $\alpha^- = \beta^- = \gamma$ . The steps for adjusting the encoding tree using the combining operator of  $\alpha$  and  $\beta$  are as follows:

- (1) Let  $T_\alpha$  and  $T_\beta$  denote the subtrees of  $\mathcal{T}$  rooted at  $\alpha$  and  $\beta$ , respectively;
- (2) Create a new node  $\delta$  with parent  $\gamma$  (i.e.,  $\delta$  shares the same parent as  $\alpha$  and  $\beta$ );
- (3) Add two child nodes to  $\delta$ :  $\delta^{(0)}$  and  $\delta^{(1)}$ ;
- (4) Insert the subtree  $T_\alpha$  and  $T_\beta$  into  $\delta^{(0)}$  and  $\delta^{(1)}$ , respectively;
- (5) Delete  $\alpha$  and  $\beta$ .

The 2-dimensional encoding tree could then be optimized to the needed  $K$ -dimension by continuing to greedily and iteratively apply merging and combining operators.

## C. Computational Complexity and Cost

This section analyzes the time complexity and computational cost of our SeSE framework to evaluate its feasibility.

1) *Computational Cost:* In terms of computational cost, model inference is involved only in the response sampling and semantic graph construction stages. The first step requires obtaining  $N$  samples, thus the original LLM needs to perform  $N$  inference operations. The second step requires using an NLI model to perform  $N^2$  bidirectional inferences to build a directed graph. Since the parameter scale of NLI models is typically much smaller than that of LLMs (e.g., the DeBERTa-large-MNLI model used in this paper has only 1.5 billion parameters), the overall computational cost is primarily determined by the number of LLM inferences in the first step. Our hyperparameter sensitivity experiments show that a relatively small sample size  $N = 5$  is sufficient to achieve strong performance, thus the actual computational cost is low. Although the sampling process introduces a minor additional expense, this cost is negligible compared with supervised methods requiring model retraining, white-box approaches dependent on internal model states, or techniques that rely

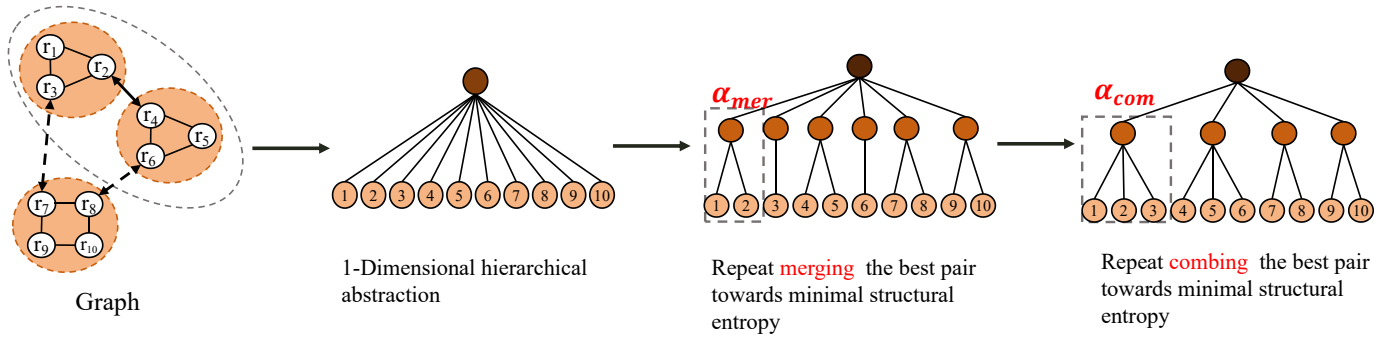


Figure 10: Illustration of the hierarchical abstracting construction.

on large and costly knowledge bases. By relying solely on sampled responses under black-box conditions, SeSE is plug-and-play and can adapt to both open-source and closed-source models, offering broader applicability.

2) *Time Complexity*: The overall time complexity of the hierarchical abstraction is  $O(n^2 + n + m \cdot \log_2 n)$ , where  $n = N = |V|$  denotes the number of vertices in the semantic graph, and  $m = |E| \approx \frac{kn}{2}$  (where  $k$  represents the out-degree per vertex in the  $k$ NN graph) indicates the number of edges retained after sparsification. The graph construction phase exhibits a time complexity of  $O(n^2 + n)$ : constructing the complete graph requires  $O(n^2)$ , and the sparsification operation requires  $O(n)$ . According to the analysis of [], the optimization process of the high-dimensional encoding tree via stretch and compression operators contributes a time complexity of  $O(m \cdot \log_2 n)$ .

#### D. Additional Experimental Details and Analysis

In this section, we provide additional experimental results.

1) *Hardware and Resources*: In terms of computing resources, as it is necessary to sample generations from LLMs to model the semantic space, our experiments require one or more GPUs to accelerate LLMs inference. Without GPU support, reproducing the results within a reasonable timeframe is infeasible. For sentence-length generation tasks, we use the GPT-5-mini model accessed through the OpenAI API to evaluate accuracy. As OpenAI’s pricing is based on the number of input and output tokens, the cost of reproducing our experiments varies with configuration, typically averaging around 1\$-5\$ per run. The concurrent experiments are conducted on two NVIDIA RTX PRO 6000 graphics cards, each with 96 GB of memory. Depending on the model and experimental setup, the generation phase for each scenario requires between 2 and 24 hours. Our experimental procedure involves first generating responses for all dataset-model pairs, followed by the computation of various uncertainty metrics. Model outputs are not regenerated across runs; instead, only the corresponding uncertainty metrics are recalculated.

2) *Assessing accuracy of automated ground-truth evaluations*: The F1 score is the harmonic mean of precision and recall of the lexical overlap between the reference answer and the generated answer. It is widely used to evaluate fixed-answer generation tasks. However, this metric exhibits obvious

limitations in sentence-length, free-form text generation: lexical overlap between LLMs responses and the short reference answers may be unreasonably low, rendering the F1 score ineffective. Therefore, our study leverages the natural language understanding capabilities of LLMs rather than relying on simple lexical matching. We employ GPT-5-mini to assess semantic equivalence between LLM-generated answers and reference answers.

To verify the reliability of our automated factual evaluation, we manually inspect 500 questions (100 from each of five experimental datasets) and analyze the sentence-length answers generated by the models. We focus on the concordance between human and automated methods, rather than the correctness of the evaluations. Table IV presents consistency statistics between automated evaluation methods and human reviewer judgments. The table shows that the agreement rate between the two human assessors (95%) closely approximates their average agreement rate with GPT-5-mini (94%). Although GPT-4o and Qwen-3-32B perform slightly worse, we select GPT-5-mini for the results presented in this paper, as it provides the best factual estimates.

3) *Assessing entailment estimator in long-form generation*: The bipartite graph construction involves entailment judgments between long-form responses and short claims. Figure 11 shows the ablation results of different entailment estimators. Conventional BERTScore and DeBERTa perform poorly, and GPT-5 does not offer notable advantages compared to GPT-5-mini. Consequently, we choose GPT-5-mini for its comparable performance and greater cost-effectiveness. The experiment is conducted on the PopQA using Gemini-2.5-Flash.

4) *Detailed results of hyperparameter sensitivity*: In Figure 12, we present the empirical statistics of semantic cluster counts across datasets used in the sentence-length experiment. As illustrated, the semantic spaces of simpler datasets such as TriviaQA and SVAMP usually contain only one or two clusters, reflecting the fact that large language models generally answer these questions correctly. In contrast, more challenging datasets like SQuAD exhibit much higher semantic complexity: approximately 30% of the questions correspond to semantic spaces with six or more clusters, indicating more intricate and disordered semantic structures. From an information-theoretic perspective, such complex semantic spaces are difficult to compress. Accurately describing them therefore requires more information (bits), i.e., constructing

Table IV: Assessing automated ground-truth evaluators.

	F1 Score	Qwen-3-32B	GPT-4o	GPT-5-mini	Human A	Human B
Human A	0.63	0.93	0.93	0.95	-	0.95
Human B	0.60	0.91	0.91	0.93	0.95	-
Average	0.62	0.92	0.92	0.94	-	-

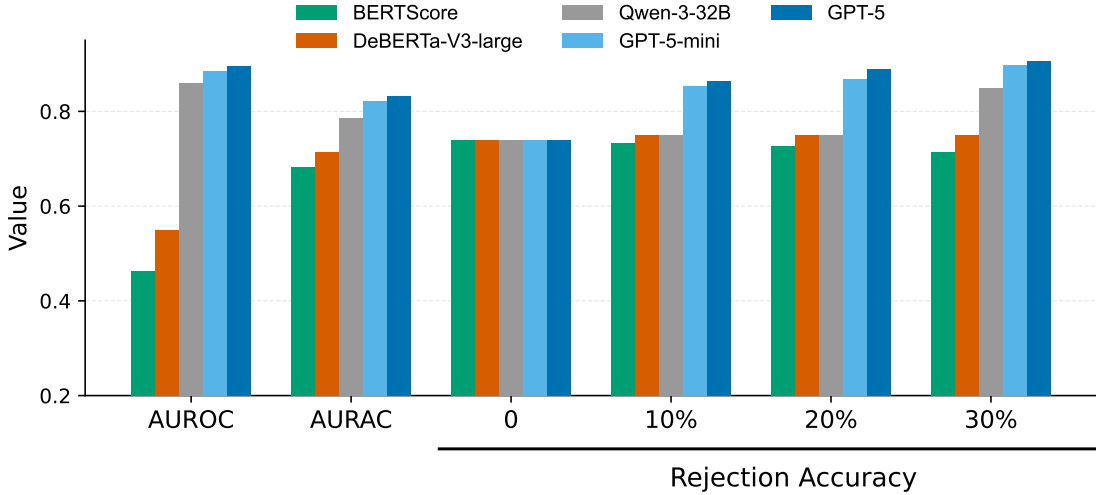


Figure 11: Assessing entailment estimators in long-form generation. The 10% rejection accuracy indicates the accuracy of the LLM after declining to respond to queries whose uncertainty ranking falls within the top 10%.

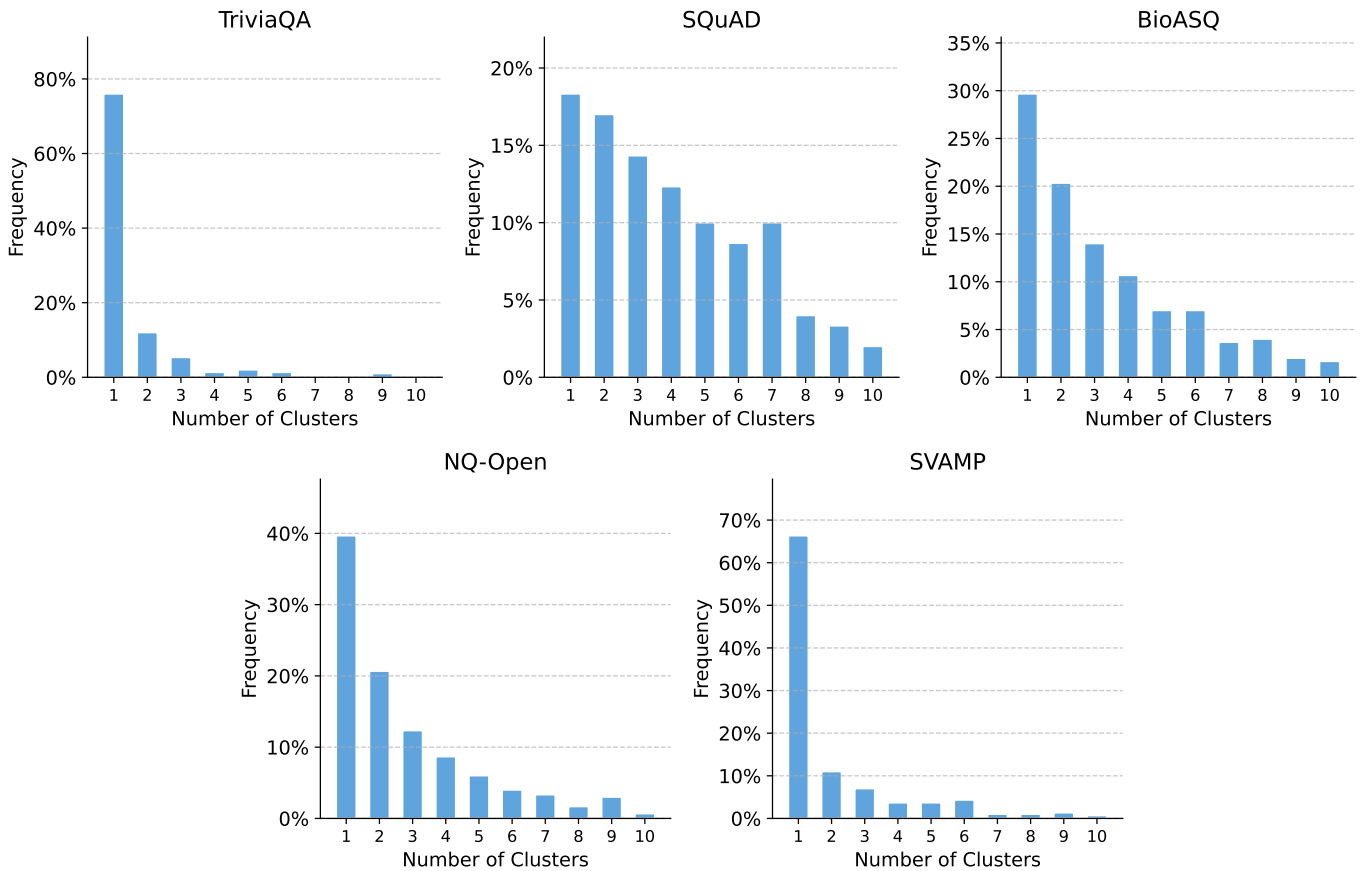


Figure 12: Statistics of semantic cluster numbers across datasets used in the sentence-length experiment. All plots are based on generations of Llama-3.1-70B.

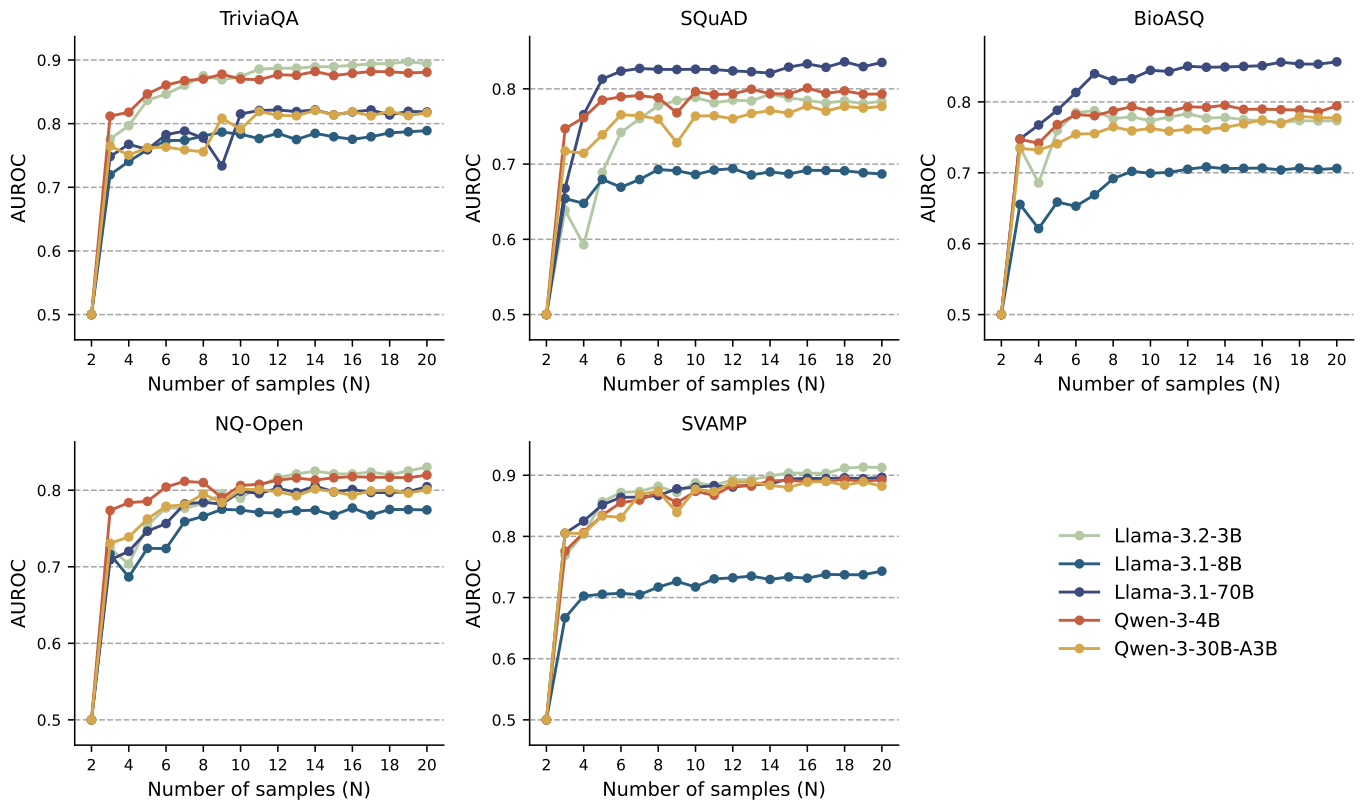


Figure 13: AUROC performance across different sample sizes in sentence-length experiments.

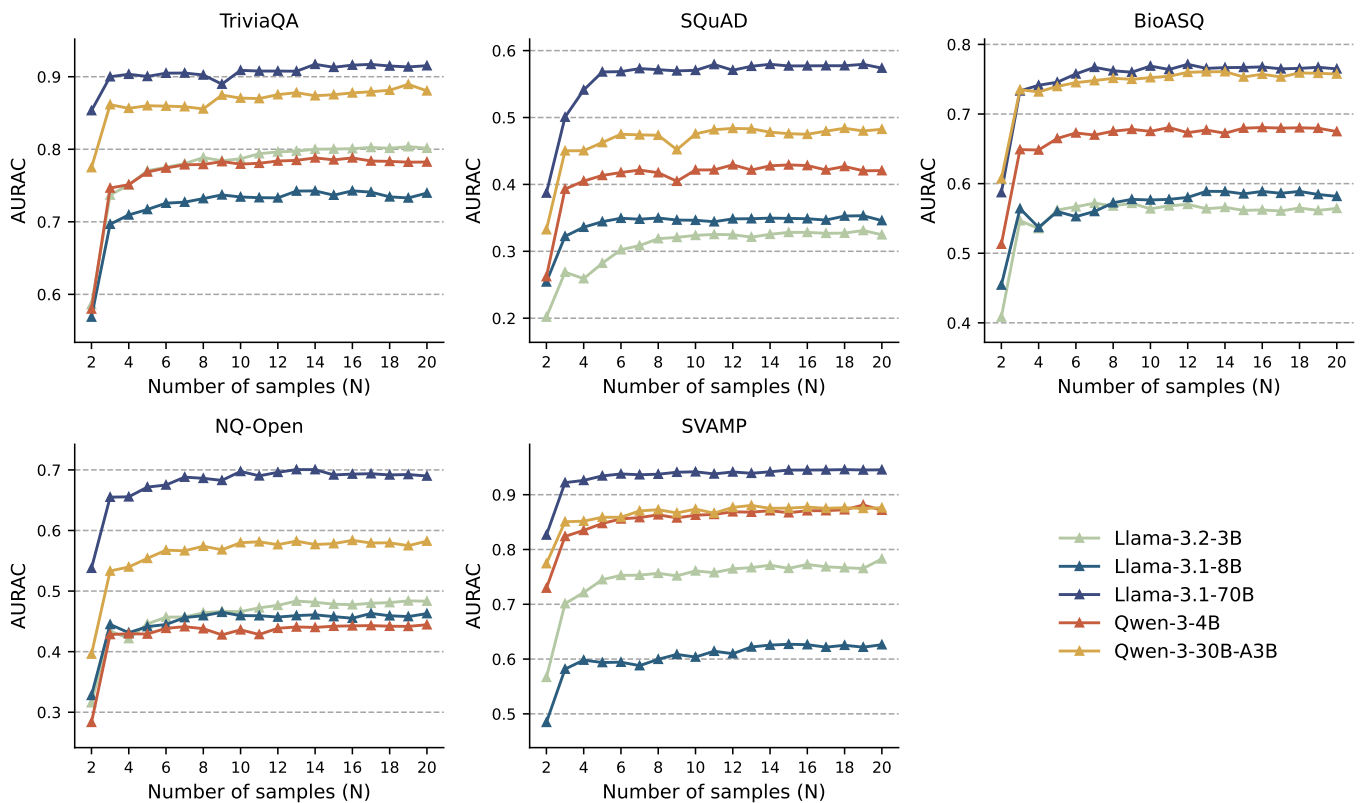


Figure 14: AURAC performance across different sample sizes in long-form experiments.

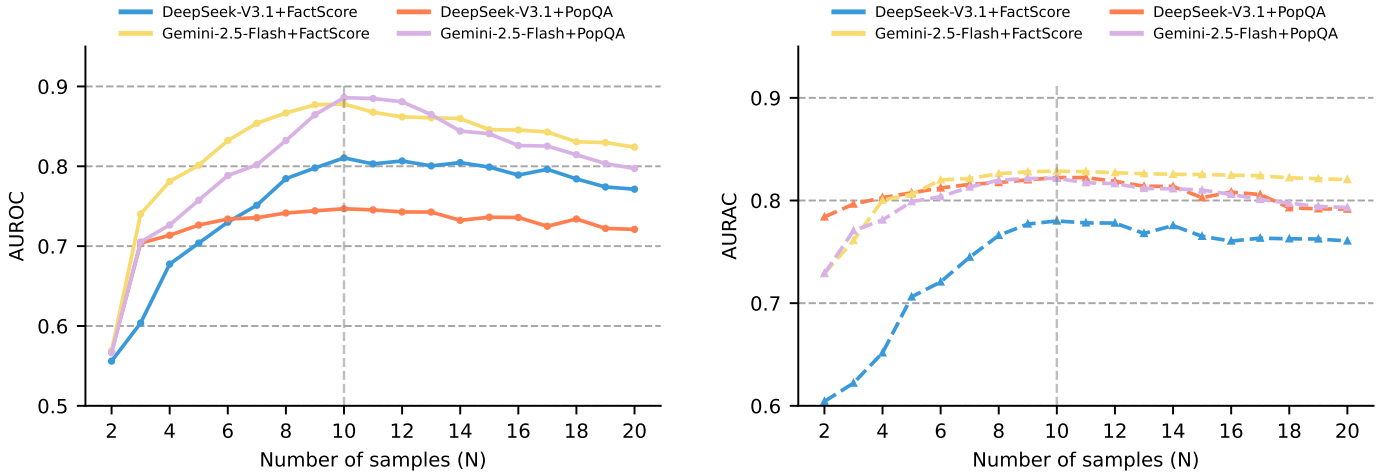


Figure 15: AUROC and AURAC performance across different sample sizes in long-form experiments.

deeper encoding trees (larger  $K$ ) to effectively quantify their inherent uncertainty.

In Figures 13—14, we report the unaggregated hyperparameter sensitivity results of the sampling size  $N$  in sentence-length experiments. Figure 15 shows the unaggregated hyperparameter sensitivity results in the long-form experiments.

#### E. Details of Case Study

Detailed information about the examples used in the case study is presented in Table V and Figure 16, based on the generations of Llama-3.1-70B on the SQuAD dataset. As shown in Figure 16, the semantic spaces of the two cases appear superficially similar: both can be divided into five semantic clusters, and the Shannon entropy values of these clusters are nearly identical. Since SE can only consider the probability distribution of semantic equivalence relations, it underestimates the uncertainty discrepancy between them, potentially leading to misjudgment. In contrast, SeSE provides a more precise assessment of uncertainty by incorporating more expressive semantic structural information. This case illustrates a representative scenario in our analysis: although the semantic spaces of the answers appear similar, intrinsic structural differences persist, and SeSE demonstrates superior performance to SE under such conditions.

#### F. Prompt Details

Here we mark **placeholders** with the orange color.

1) *Response sampling prompt*: For sentence-length experiments, we use the following generation template:

*Answer the following question concisely in one complete sentence.*

*Question: {question}*

*Answer:*

2) *Claim decomposition prompt*: Given a LLM response, the claim decomposition prompt is used to break down the generated response into a set of individual claims. The prompt is as follows:

*You will be provided with a long-form text that contains multiple claims. A claim is the smallest independent and*

*self-contained perspective. Your task is to precisely identify and extract each claim within the given text, making sure there is no semantic repetition. Then, for the sake of clarity, resolve all anaphora (pronouns or other referring expressions) within the claims. Each claim should be concise and independently complete. Ensure that you are comprehensive and list each claim as a separate sentence.*

*The input is: {greedily decoded response}*

*Output:*

3) *Ground-truth evaluation prompt*: For sentence-length generation, we automatically determine whether the given answer is correct or incorrect by comparing it with the reference answer using GPT-5-mini. We use the following template:

*We are evaluating the correctness of answers to the question: {question}*

*The reference answer is: {reference answer}*

*The proposed answer is: {greedy decoding generation}*

*According to the reference answer, determine whether the proposed answer is correct within the context of the question. Respond with only Yes or No.*

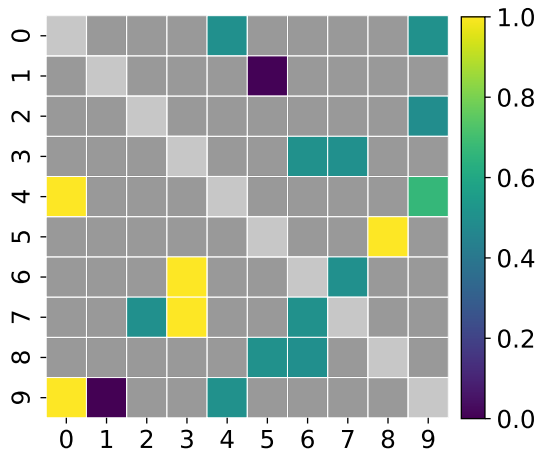
For the dataset SQuAD\_V2 with multiple reference answers, the second line becomes “The following are the reference answers:”, and the last line asks “determine whether the proposed answer has the same meaning as any of the reference answers within the context of the question.”

#### G. Dataset and Annotation Details

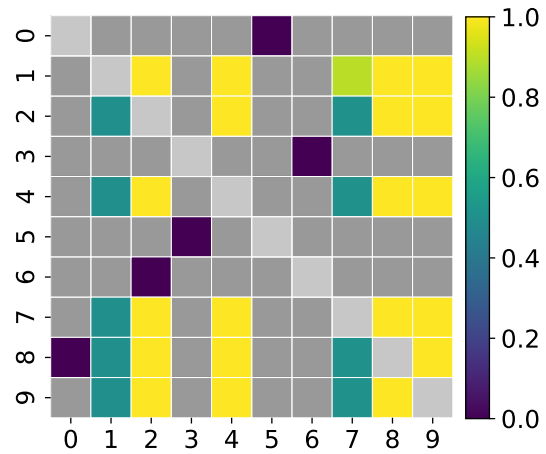
SeSE can detect confabulations in free-form text generation across a range of domains without requiring prior domain knowledge. We evaluate it on sentence-level question-answering tasks spanning life sciences, mathematical reasoning, trivia knowledge, open-domain QA, and common-sense reasoning. Furthermore, to examine SeSE’s hallucination detection capability in long-text generation tasks, we construct four custom datasets based on the generated outputs of DeepSeek-V3.1 and Gemini-2.5-Flash on two benchmark datasets—FActScore and PopQA. Since current LLMs have an excessively high accuracy rate when using tools, all experiments are conducted in offline mode, relying solely on

Table V: Examples from SQuAD that are generated by Llama-3.1-70B.

Hallucination case
Question: What spacecraft contained data to determine the oxygen content of the Sun? Answer: Genesis spacecraft Sampled Responses: 1. Mariner 2 contained data to determine the oxygen content of the Sun. 2. Helios 1 and 2 contained data to determine the oxygen content of the Sun. 3. The Helios spacecraft contained data to determine the oxygen content of the Sun. 4. The Mars Global Surveyor contained data to determine the oxygen content of the Sun. 5. The Helios spacecraft contained data to determine the oxygen content of the Sun. 6. The Apollo 15 command module contained data to determine the oxygen content of the Sun. 7. The ACRIM-1 experiment was used to determine the oxygen content of the Sun. 8. Helios 1 contained data to determine the oxygen content of the Sun. 9. Helios contained data to determine the oxygen content of the Sun. 10. The Helios spacecraft contained data to determine the oxygen content of the Sun.
Non-hallucination case
Question: What gearing was used on steam turbine marine engines in the 20th century? Answer:reduction Sampled Responses: 1. In the 20th century, steam turbine marine engines often used reduction gearing to connect the turbine to the propeller shaft. 2. In the 20th century, single or double helical gearing was used on steam turbine marine engines. 3. In the 20th century, the gearing on steam turbine marine engines typically had pinions with 8 to 13 teeth and wheels with 60 to 100 teeth, with gear ratios usually around 5:1 to 7:1. 4. In the 20th century, most steam turbine marine engines used single reduction gearing, although a few used double reduction or triple reduction gears. 5. In the 20th century, steam turbine marine engines typically used one or more sets of reduction gears, along with one or more steam turbines, including power turbines and condensing turbines, to drive the propeller shaft. 6. In the 20th century, steam turbine marine engines used reduction gearing and epicyclic gearing. 7. In the 20th century, most steam turbine marine engines used single-reduction gearing, although some triple-expansion and other reciprocating steam engines used double-reduction gearing. 8. In the 20th century, most steam turbine marine engines used single reduction gearing with double helical gears on a single pinion; some US Navy ships used triple reduction gearing, some merchant ships and submarines used a combination of gearing and a fluid coupling, the British Royal Navy used double reduction gearing, and some high-speed, high-powered ships used triple reduction gearing or single reduction with a fluid coupling, while some smaller ships and submarines used single reduction without a fluid coupling, making single reduction with double helical gears the most common gearing. 9. In the 20th century, steam turbine marine engines used epicyclic gearing. 10. In the 20th century, gearing on steam turbine marine engines typically involved a combination of a high-pressure turbine and a low-pressure turbine connected to a reduction gear that drove the propeller shaft.



(a) Heat map of the adjacency matrix that models the semantic space of the used hallucination cases.



(b) Heat map of the adjacency matrix that models the semantic space of the used non-hallucination cases.

Figure 16: The visualization of semantic spaces that is used for case study.

Table VI: Details of sentence-length experiment datasets.

Dataset (Linked)	Domain	Count	Example question	Context	Answer
BioASQ	Life sciences	4.7k	What disease is the ALK tyrosine kinase associated with?	*Discard	Cancer.
SVAMP	Mathematical word problems	1k	How many white t-shirts will she have?	If mom buys 57 packages of white t-shirts and 34 trousers. White t-shirts can be purchased in packages of 53.	3021.
TriviaQA	Trivia knowledge	15.4k	Claude Littner is the new face in the latest series of which programme?	*Discard	Apprentice.
NQ-Open	Open-domain natural questions	91.5k	The removal of temperature in fire fighting method is known as?	*Discard	Cooling.
SQuAD	General knowledge	141.9k	When was Otto von Bismarck born?	*Discard	1862.
FactScore	Biographies	3.5k	Tell me a bio of Maxime Masson.	—	—
PopQA	Multi-topic Wikipedia entries	3.8k	Provide me with a paragraph detailing some facts related to Speak (2004 film).	—	—

\*Discard denotes that we don’t include context in prompts.

their own capabilities. In Table. VI, we show samples and statistics for each dataset. All experimental datasets have been made publicly available in the code repository to facilitate reproducibility and further development.

1) *Datasets in sentence-length experiments:* In the sentence-length experiment, we utilize five representative QA datasets covering different domains: BioASQ [37], SVAMP [38], TriviaQA [39], NQ-Open [40], and SQuAD\_V2 [41]. BioASQ derives from the annual biomedical semantic-indexing and question-answering challenge of the same name, focusing on life sciences. We select dataset from Task B of the 2023 BioASQ challenge. SQuAD\_V2, a reading comprehension dataset, contains answers extracted from Wikipedia paragraphs. We exclude unanswerable questions designed to induce erroneous responses. TriviaQA encompasses trivia questions across multiple domains, including history, science, entertainment and so on. SVAMP features elementary mathematical word problems that test reasoning abilities. NQ-Open, an open-domain subset of Natural Questions, comprises real Google search queries with answers found in Wikipedia documents.

For each dataset, we sample 300 examples for training and 300 for testing each time with different random seed. Notably, SeSE is completely independent of the training data. For datasets with predefined partitions, sampling occurred within their respective training and test sets. All experiments employ free-form question answering rather than multiple-choice or true/false formats to better assess the characteristics of LLMs in generating free-form text. As the questions become too easy for the current LLMs when context is provided, we withhold context paragraphs across all experiment datasets except SVAMP to increase difficulty and provoke potential hallucinations.

2) *Datasets in long-form experiments:* We select DeepSeek-V3.1 and Gemini-2.5-Flash as representative SOTA LLMs at the time of writing. Due to the absence of fine-grained, long-form hallucination evaluation datasets for these two models, we construct four new datasets based on entities from FActScore [27] and PopQA [42].

**FActScore:** This dataset is widely used for evaluating the factuality of biographies generated by LLMs, with entities sourced from Wikipedia. We select entities from the publicly released “unlabelled” portion and prompt each model with

the query “Tell me a bio of [subject]” to collect long-form generations.

**PopQA:** This dataset contains Wikipedia entries spanning 16 subject domains. Although PopQA is not originally designed for long-text generation, it includes long-tail entities with low-popularity, which present substantial challenges for offline-deployed LLMs. We filter for long-tail entities and prompt each model with the query “Provide me with a paragraph detailing some facts related to [subject]” to collect model-generated content.

To ensure quality, we further filter entities based on the informational completeness of their corresponding Wikipedia pages, removing those with page lengths shorter than 2000 tokens. This step ensures that each retained Wikipedia page contains sufficient reference material for subsequent annotation.

**Annotation Process:** For each model-dataset pair (four pairs in total), we employ a two-stage cross-validation annotation process. First, we generate factual claims for each sampled entity, following the processing pipeline detailed in Section III-C. Each claim is then evaluated for factual accuracy according to the following criteria:

- **True:** The claim is factually accurate and can be verified by the corresponding Wikipedia page.
- **False:** The claim contains factual errors or contradicts information found on the corresponding Wikipedia page.

To enhance annotation efficiency and consistency, we utilize two powerful reasoning models, GPT-4 and DeepSeek-R1, for automated labeling. A claim is automatically assigned a label only if both models produce identical classifications; otherwise, the claim is reviewed by human annotators for final decision. This hybrid annotation framework ensures high accuracy while enabling large-scale processing. In total, **7,407** generated claims have been annotated through this process.

We find that even such powerful LLMs exhibit significant hallucination rates, with 28% for DeepSeek-V3.1 and 27% for Gemini-2.5-Flash. Although hallucinations, like software vulnerabilities, cannot be completely eliminated at the current stage, effective detection mechanisms can mitigate associated risks and enhance the reliability of LLMs. Given that hallucinations may lead to serious real-world consequences, reliable uncertainty quantification is crucial for ensuring the responsi-

ble deployment of LLM-based systems, which highlights the important value of our research.

### H. Baselines Details

This section aims to comprehensively elaborate on the benchmark methods employed in our experiments. We will conduct an in-depth analysis of the specific details of each method, including its prompts and implementation approaches. By providing detailed descriptions of these benchmark methods, we strive to ensure the reproducibility and transparency of the experimental setup.

#### 1) Baselines in sentence-length experiments

**Embedding Regression (ER)** [24]. Embedding Regression represents the typical supervised learning approach. Kadavath et al. [24] develop predictors by fine-tuning proprietary language models on annotated QA datasets to assess whether target LLMs could correctly answer specific questions. Our experiment implements a more efficient alternative: we directly extract the final hidden layer states from LLMs and train a Embedding Regression classifier to achieve equivalent predictive functionality without requiring model fine-tuning or ground-truth answers.

**P(True)** [24]. This method first prompts LLMs to generate multiple distinct answers, then presents this answer list alongside the greedy decoding response and a binary question: “Is this answer (a) correct or (b) incorrect?”. The confidence score is derived from the probability with which the model selects option “(a)”. We enhance P(True) through few-shot prompting by incorporating ten randomly selected training examples formatted according to the described protocol and annotated with their true labels. This strategy represents a form of supervised in-context learning that leverages partial ground truth without necessitating model retraining.

**Length-normalized Predictive Entropy (LN-PE)** [47]. To calculate prediction entropy, we must obtain the probabilities that LLMs assign to generated token sequences. The probability of an entire sequence  $s$  given context  $x$  equals the product of probabilities for each token conditioned on previous tokens, with its log probability expressed as  $\log P(s|x) = \sum_i \log P(s_i|s_{<i}, x)$ .  $s_i$  is the  $i$ -th output token and  $s_{<i}$  denotes all preceding tokens. Due to the conditional independence of token probabilities, longer sequences inherently have lower joint likelihood. The joint likelihood of a sequence decreases exponentially with length  $L$ , while its negative log probability increases linearly with  $L$ , causing longer sentences to contribute disproportionately to entropy. Length-normalized prediction entropy addresses this bias by normalizing the log probability by sequence length, using the arithmetic mean  $\frac{1}{L} \sum_{i=1}^L \log P(s_i|s_{<i}, x)$ . This normalization effectively assumes that the uncertainty of the generated result is independent of sequence length.

**Semantic Entropy (SE) and Discrete Semantic Entropy (DSE)** [14], [16]. Semantic entropy aims to evaluate the uncertainty of LLMs regarding the meaning of their generated sequences. It first calculates the sum of probabilities for all token sequences that can be considered as expressing the same meaning. Given context  $x$ , for each semantic equivalence

class  $c$ , its probability  $P(c|x)$  is estimated through semantic clustering of generated sequences  $s$ :

$$P(c|x) = \sum_{s \in c} P(s|x) = \sum_{s \in c} \prod_i P(s_i | s_{<i}, x). \quad (23)$$

Semantic entropy (SE) is then estimated as the Shannon entropy of the meaning distribution:

$$SE(x) = - \sum_{c \in \mathcal{C}} P(c|x) \log P(c|x). \quad (24)$$

In practice, it is not possible to calculate  $\sum_C p(C|x) \log p(C|x)$  because of the intractable number of semantic clusters. Instead, discrete semantic entropy (DSE) uses a Rao-Blackwellized Monte Carlo estimator

$$DSE(x) \approx - \sum_{i=1}^M p'(C_i|x) \log p'(C_i|x), \quad (25)$$

where  $C_i$  are  $M$  clusters extracted from the  $N$  generations and  $p'(C_i|x) = \frac{p(C_i|x)}{\sum_k p(C_k|x)}$ , which we refer to as  $p(C_i|x)$  in the following for simplicity. DSE can be extended to cases where token likelihoods are not available by approximating  $p(C_i|x)$  with the fraction of generated texts in each cluster,  $p(C_i|x) \approx \sum_{i=1}^N \mathbb{I}(s_i \in C_i) / N$ .

**Kernel Language Entropy (KLE)** [17]. To address the limitations of traditional semantic entropy, which only rely on semantic equivalence relations and fail to capture fine-grained semantic similarities, Nikitin et al. proposed Kernel Language Entropy (KLE). It encodes the semantic similarities between texts generated by LLMs through a unit trace positive semidefinite kernel  $K_{\text{sem}}$ , and then use the von Neumann Entropy (VNE) to quantify the uncertainty of the semantic space represented by this kernel. For a unit trace positive definite matrix  $A \in \mathbb{R}^{n \times n}$ , its von Neumann Entropy, denoted as  $VNE(A)$ , is defined in the form of matrix trace operation. On this basis, the KLE is defined as the VNE of the semantic kernel:

$$VNE(A) = -\text{Tr}[A \log A], \quad (26)$$

$$KLE(x) = VNE(K_{\text{sem}}). \quad (27)$$

**SelfCheck-Prompt (SC-Prompt)** [25]. SC-Prompt represents the highest-performing variant within the SelfCheckGPT framework. Its central idea is to prompt the LLM to assess the semantic consistency between the target sentence and a set of randomly generated samples, thereby determining the presence of hallucinations. The procedure is as follows: given a sentence to be evaluated  $r_i$  and  $N$  randomly generated samples  $S^n$  corresponding to the same query, a fixed prompt template is used to instruct the LLM to evaluate their semantic consistency. The LLM’s output is then converted into a numerical score  $x$  in accordance with predefined rules. Finally, the inconsistency score for the sentence is obtained by averaging these individual scores. A score approaching 1.0 indicates a higher likelihood that the sentence contains hallucinations. The calculation formula is:

$$SC_{\text{Prompt}} = \frac{1}{N} \sum_{n=1}^N x^n, \quad (28)$$

where  $x_i^n$  is the mapping score corresponding to the  $n$ -th sample.

### 2) Baselines in long-form experiments

**Discrete Semantic Entropy (DSE) variant [16].** For long-form generation, discrete semantic entropy operates through three key steps: (1) decomposing the text into atomic claims, (2) generating multiple possible questions that could trigger each claim in reverse, and (3) querying the original LLMs to produce new responses for each question, while including the original claim as a candidate. The final uncertainty estimate for each claim is derived by averaging the semantic entropy values across all associated questions. In our long-form experiments, we implement discrete semantic entropy according to the original paper’s best practices. Applying discrete semantic entropy to long-form generation introduces additional assumptions and complexities, and its computational cost increases with higher sampling. In contrast, SeSE achieves better performance with a more concise principle and lower cost.

**Verbalized confidence (VC) [22].** Verbalized Confidence prompts LLMs to directly express their confidence in a claim through natural language. Uncertainty is quantified by parsing the confidence expressions in the LLMs’ output (e.g., “very confident”, “100%”, etc.) and mapping them to numerical values. Here, we mainly consider two variants:

**Post-hoc Verbalized Confidence (PH-VC):** This method elicits the verbalized confidence in a post-hoc manner after the entire claim set  $C$  has been decomposed from generations. Specifically, we prompt an LLM to express its confidence about each claim  $c \in C$  given multiple options such as “Unlikely (40%)”, “Even chance (50%)” etc. The specific prompt that we use is as following:

*You are provided with some possible information about a Wikipedia entity. Assess the likelihood that this information is correct and describe it using one of the following expressions: Certainly false (0%), Very unlikely (20%), Unlikely (40%), Even chance (50%), Possibly true (60%), Likely (80%), Certainly true (100%).*

*Just provide your confidence expression, do not output other text or explanations.*

*The entity is: {entity}*

*The possible information is: {claim}*

*Output:*

**In-line Verbalized Confidence (IL-VC):** In-line verbalized confidence (IL-VC) directly elicits the verbalized confidence about each claim  $c$  in an in-line manner right after it is decomposed from the generations. Thus, we prompt LLMs with a long-form generation and instructions to give all the claims with corresponding confidence scores. The specific prompt that we use is as following:

*Please deconstruct the input paragraph into the smallest possible standalone self-contained facts without semantic repetition with corresponding confidence score.*

*The confidence score should represent your confidence in the claim, where a 1 is obvious facts and results like  $1+1=2$ . A 0 represents claims obviously incorrect or difficult for anyone to understand, such as “The Earth is the center of the universe” or “The exact population of a certain ordinary*

*town”.*

*You must return the output as a jsonl, where each line is claim: {[claim],[confidence score]}.*

*The input is: {long-form generation}*

*Output:*

**P(True) variant.** P(True) estimates the uncertainty of a claim by prompting LLMs to answer whether a claim is true or false, using the probability of the claim being true as the confidence score. Since probabilities cannot be obtained directly in long-form experiments, we improve this method by prompting the model to answer 10 times and estimating the probability by calculating the frequency of “true” responses. The specific prompts we use are as follows:

*Is the claim true or false? Answer with only True or False.*

*Claim: {claim}*

*Output:*

**SC-Prompt variant.** This methods utilizes the consistency score of one claim across different samples. The consistency score is determined by prompting the same LLM.

**Graph Centrality Metrics [19].** By integrating information theory with graph analysis, SeSE offers a principled measure of network structural disorder and establishes a computational paradigm for hierarchical abstraction. To validate SeSE’s advantages in quantifying intra-graph information, we compare it against various widely used graph-based analysis metrics. The specific definitions of these baseline metrics are detailed in Table VII, including Betweenness, Eigenvector, PageRank and Closeness.

Table VII: Benchmark graph centrality metrics with their formulas and explanations.

Metric	Formula	Brief Explanation
Betweenness	$C_B(v) = \sum_{s \neq v \neq t} \frac{\sigma_{st}(v)}{\sigma_{st}}$	Fraction of shortest paths $\sigma_{st}$ between other nodes $s, t$ that pass through a node $v$ .
Eigenvector	$C_{Eigv}(v) = \frac{1}{\lambda} \sum_{u \in N(v)} A_{vu} C_{Eigv}(u)$	Evaluates the influence of node $v$ based on the importance of its neighbors $N(v)$ . $A_{vu}$ is adjacency matrix entry. $\lambda$ is the largest eigenvalue of the adjacency matrix.
PageRank	$C_{PR}(v) = \frac{1-d}{ V } + d \sum_{u \in N(v)} \frac{C_{PR}(u)}{ N(u) }$	Quantifies node importance by combining link quantity and quality. $d$ is the damping factor. $N(v)$ is the set of neighboring nodes of node $v$ .
Closeness	$C_C(v) = \frac{ V -1}{\sum_{u \in V} d(v,u)} \cdot \frac{ V }{ V_v }$	Reciprocal of the average shortest path distance to all nodes. $d(v, u)$ is the shortest-path distance between $v$ and $u$ . $ V_v $ is number of nodes reachable from $v$ .

$V$ : The node set of graph  $G$ .  $A$ : The adjacency matrix of graph  $G$ .  $|V|$ : The total number of nodes in graph  $G$ .

Table VIII: The formulas and explanations of graph uncertainty metrics used in ablation study.

Metric	Formula	Brief Explanation
Eingvalue	$U_{Eigv} = \sum_{k=1}^m \max(0, 1 - \lambda_k)$	Quantifies graph uncertainty by summing positive differences between 1 and each Laplacian matrix eigenvalue $\lambda_k$ , reflecting structural instability.
Degree	$U_{Deg} = \frac{\text{trace}( V I - D)}{ V ^2}$	Measures graph uncertainty through normalized difference between ideal connectivity (scaled identity matrix $ V I$ ) and actual connectivity (degree matrix $D$ ).
Eccentricity	$U_{Ecc} = \frac{1}{m} \sum_{i=1}^m \ v_i - \bar{v}\ _2$	Captures graph uncertainty via average Euclidean distance between node embeddings $v_i$ and their mean $\bar{v}$ , with larger distances indicating higher uncertainty.
Spectral Gap	$U_{Spec} = 1 - \lambda_2$	$\lambda_2$ is the second smallest eigenvalue of the Laplacian matrix of $G$ . Smaller $\lambda_2$ indicates weaker connections and higher uncertainty. $U_{Spec}$ inverts $\lambda_2$ to ensure that larger values reflect greater uncertainty.

$V$ : The node set of graph  $G$ .  $A$ : The adjacency matrix of graph  $G$ .  $|V|$ : The total number of nodes in  $G$ .